Politecnico di Torino

Departamento di Energia

Study of Chemical Looping and later applications

Carlos Escribano Sanz

Tutor: Pierluigi Leone

Index

Abstract .....

1. Chemical Looping ..... ¡Error! Marcador no definido.

1.1. What is Chemical Looping? ..... **¡Error! Marcador no definido.**

1.2. Chemical Looping examples ..... **¡Error! Marcador no definido.**

1.2.1. Chemical Looping Combustion 1

1.2.2. Chemical Looping Reforming 3

1.3. Other studies done about Chemical Looping 3

1.3.1. Computational Fluid Dynamic studies (CFD) of CLC 3

1.3.2. Calcium and Iron Oxide Reactivity Studies for Chemical Looping **¡Error! Marcador no definido.**

1.3.3. Mechanistic studies of Chemical Looping 5

1.4. Thesis' study of the Chemical Looping 5

1.5. Syngas Chemical Looping (study's Chemical Looping) 5

2. Modelling of Study's Chemical Looping Cycle **7**

3. Analysis of the three reactors **9**

4. Aspen Plus technology **11**

4.1. Elements used in the thesis' cycle ..... **¡Error! Marcador no definido.**2

5. Simulation of Chemical Looping cycle ..... ¡Error! Marcador no definido.**3**

5.1. Simulation ..... **¡Error! Marcador no definido.**3

5.2. Conclusions ..... **¡Error! Marcador no definido.**4

6. Applications of Chemical Looping technologies ¡Error! Marcador no definido.**5**

6.1. Hydrogen storage and Onboard Hydrogen Production **¡Error! Marcador no definido.**5

6.1.1. Compressed Hydrogen gas and Liquefied Hydrogen 15

6.1.2. Metal Hydrides 17

6.1.3. Bridged Metal-Organic Frameworks 18

6.1.4. Carbon Nanotubes and Graphite Nanofibers 19

6.1.5. Onboard Hydrogen Production via Iron Based materials 20

6.2. Carbonation-Calcination Reaction (CCR), Carbon Dioxide capture 28

6.3. Chemical Looping Gasification Integrated with Fuel Cells 34

6.3.1. Chemical Looping Gasification Integrated with Solid-Oxide Fuel Cells ..... 3**¡Error! Marcador no definido.**

6.3.2. Direct Solid Fuel Cells 36

6.4. Enhanced Steam Methane Reforming..... 38

6.5. Tar Sand Digestion via Steam Generation 40

6.6. Liquid Fuel Production for Chemical Looping Gasification..... 40

6.7. Chemical Looping with Oxygen Uncoupling (CLOU) 41

6.8. Concluding Remarks..... 44

References 45

Figures

1.1. Chemical Looping Combustion Scheme....2

1.2. Chemical Looping Reforming Scheme....3

2.1. Study's Chemical Looping Scheme....7

3.1. Molar flow-Temperature Graphic Oxidizer....9

3.2. Molar flow-Temperature Graphic Combustor....10

3.3. Molar flow-Temperature Graphic Reducer....10

4.1. Aspen plus flowsheet....12

4.2. Reactors....12

4.3. Separators....13

5.1. Study's Chemical Looping Cycle in Aspen Plus....13

5.2. Results of the simulation by steams....14

6.1. Gravimetric and volumetric energy densities of various hydrogen storage....16

6.2. Overall scheme of using Fe modules to produce hydrogen on a vehicle....22

6.3. Designs for reactors with Fe containing media: packed bed of small pellets; monolithic bed with straight channels for steam; and monolithic bed with channels for steam and air....23

6.4. H_2 production module using a series of fixed - bed reactors....24

6.5. H_2 production module using a series of monolithic - bed reactors....24

6.6. H_2 production module using a series of monolithic - bed reactors with air injection to provide heat for steam formation....25

6.7. System integration for use of Fe module with a H2 ICE using, (a) water to cool the ICE and (b) a high - temperature coolant to cool the ICE....26

6.8. Hydrogen production from a stand - alone Fe module....27

6.9. CO2 Capturing and Separation Scheme....29

6.10. Effect of Ca:C molar ratio on the CO2 removal efficiency for three Ca -based sorbents....29

6.11. Effect of Ca:C molar ratio on the SO_2 removal efficiency for three Ca - based sorbents....30

6.12. Relationship between the parasitic energy consumption and PCC sorbent molar conversion efficiency. 30

6.13. Conceptual schematic of Carbonation – Calcination Reaction (CCR) Process integration for a 300 - MWe (900 - MWth) coal - fi red power plant depicting heat integration strategies 31

6.14. Subpilotscale - CCR Process facility located at The Ohio State University 32

6.15. Internal view of the U - bend section of the subpilot - scale facility (given in Figure 6.14) after one week of operation 33

6.16. Results of the CO 2 removal efficiency from Ohio State University cyclic testing of calcium hydroxide at a Ca:C molar ratio of 0.75 33

6.17. Chemical looping gasification integrated with a solid - oxide fuel cell 34

6.18. Direct solid - oxide fuel cell applications for chemical looping 36

6.19. Schematic flow diagram of the chemical looping combustion integrated with the steam methane-reforming process (CLC – SMR) 38

6.20. Heat and steam generation by the looping process 40

6.21. Chemical looping gasifi cation for liquid fuel synthesis 41

6.22. Partial pressure of gas-phase O2 over metal - oxide systems as a function of temperature. CuO/Cu2O (—); Co3O4 /CoO (– – –) Mn2O3 /Mn3O4 (- - -) 42

6.23. Laboratory fluidized - bed reactor used for solid - fuel CLOU testing by Chalmers University 43

Tables

6.1. Coal - to - Electricity Process Confi gurations and Process Efficiencies 35

The Ideal Cell Potentials (Open - Circuit Voltage) 37

6.3. Performance Comparisons of Conventional CTL and Chemical -Looping - Gasifi cation - Based CTL ..... 4**¡Error! Marcador no definido.**

6.4. Solid Fuels Testing Results Using the CLOU Concept: Copper-BasedMetal Oxide vs. Iron-Based Metal Oxide 44

Abstract

In this project the goal is to prove the efficiency of the chemical looping, after explaining in what consist and which are its principal uses, and explain the most important applications that use this thermodynamical cycle to improve the work and achievements.

To make the study it has been used the simulation program named ASPEN PLUS. After modeling the cycle in the program and running the simulation, it has been seen that is efficient and its helpful to bigger cycles that share a common goal.

In the applications explained after, it’s seen that the chemical looping really improves the processes that have required it.

1. Chemical Looping

1.1. What is chemical looping?

Chemical looping, a low carbon technology for the fossil fuel industry, is increasingly been viewed as a competitive technology in carbon capture and storage.

As the world increasingly transitions to a low-carbon economy, it is becoming important for fossil fuel-based industries to develop ways to reduce their carbon dioxide (CO_2) emissions. To do this many fossil fuel-based industries, and in particular coal-based power stations, are promoting carbon capture and storage (CCS). This is where the CO_2 generated from coal combustion is separated from the power station's flue gas and sequestered for long-term storage. The advantage of CCS is that it enables existing infrastructure and industries to meet carbon emission reductions while continuing to operate into the medium-term future.

In CCS, one of the key technology barriers is developing separation technologies that can produce a pure CO2 product for sequestration. Currently, most approaches focus on separating CO2 from the flue gas being emitted from a power station's chimney.
This is an energy intensive approach, as they are trying to separate CO_2 from a range of other gases, such as nitrogen, oxygen and water vapor. Hence, up to 25% of the power station's output can be required to separate and purify the CO_2 gas. This is known as the CCS parasitic load on the power station, and the major focus of current CCS research is to reduce the parasitic load as much as possible.

1.2. Chemical Looping examples

1.2.1. Chemical Looping Combustion

Chemical looping combustion (CLC) dates from the early 1980's when it was proposed as a system for augmenting power station efficiency. CLC works in a simple manner: instead of performing hydrocarbon combustion in a single reaction stage, two (or conceivably more) reactions are used. An additional species is required, which re-circulates between the two reactions carrying oxygen atoms. This additional species is called the oxygen carrier and is typically a metal. As an example, consider the following two reactions using a nickel based reaction scheme

$$2Ni_{(s)} + O_2 \rightarrow 2NiO_{(s)} \quad (1)$$

$$C_{(s)} + 2NiO_{(s)} \rightarrow CO_{2(g)} + 2Ni_{(s)} \quad (2)$$

If reactions (1) and (2) are added together the nickel simply re-circulates between the two reactions, hence, from the perspective of an overall mass and energy balance, the two reactions simplify to the basic carbon oxidation reaction, thus:

$$C_{(s)} + O_{2(g)} \rightarrow CO_{2(g)}$$

Both reactions (1) and (2) are arranged to take place in separate vessels called, respectively: the oxidizer and reducer (or air reactor and fuel reactor). This leads to a key advantage of CLC: In conventional power stations, since the fuel is burned in the presence of air, the CO2 inevitably becomes diluted with nitrogen necessitating an expensive post-combustion scrubbing system. As a result, carbon capture is often seen as both energetically and economically unattractive. However, this problem is circumvented in CLC since the fuel enters the reducer rather than the oxidizer. As a result, the fuel never comes into contact with air, and therefore the CO2 produced in the system remains undiluted with nitrogen.

However, avoiding a post combustion scrubbing plant is not the only advantage of CLC; it can improve power station efficiency too. To illustrate this, the figure below shows a schematic diagram of a CLC plant and includes a Sankey diagram of the flow of energy. Studying the diagram below, a heat engine straddles the two reaction vessels. The oxidation reaction is arranged to be highly exothermic producing a heat flux at a high temperature – this flux is used to drive a heat engine. The heat engine, in turn, must reject heat, which it does at medium temperature into the reducer. The reduction reaction is arranged to be endothermic and it is the heat rejected by the heat engine that drives this reaction.

Why does this process enable the thermal efficiency to be increased? Careful selection of the oxygen carrying species enables the equilibrium temperature of the two redox reactions to be reduced below current metallurgical limits. Consequently, using CLC it is theoretically possible to approach a reversible IC engine without resorting to impractical temperatures. Critically, CLC achieves this increase in efficiency using the same 'chemical plant' that is used to capture CO2; the capital equipment used to capture CO2 is also used to increase power station performance.

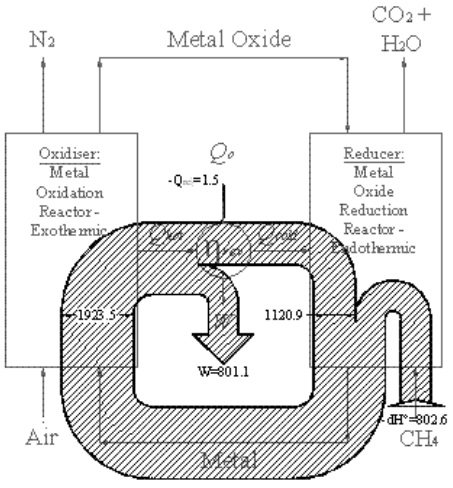

Figure 1.1. Chemical Looping Combustion Scheme

1.2.2. Chemical Looping Reforming

Chemical-looping reforming (CLR) utilizes the same basic principles as CLC, being the main difference that the wanted product in CLR is not heat but H2 and CO. Therefore, in the CLR process the air to fuel ratio is kept low to prevent the complete oxidation of the fuel to CO2 and H2O. An important aspect to be considered in a CLR system is the heat balance. The oxidation reaction of the metal oxide is very exothermic, however, the reduction reactions are endothermic. So, the heat for the endothermic reduction reactions is given by the circulating solids coming from the air reactor at higher temperature. The heat generated in the air reactor must be enough high to fulfil the heat balance in the system.

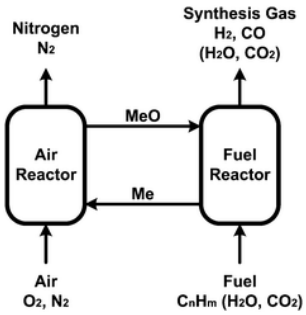

Figure 1.2. Chemical Looping Reforming Scheme

Due to reaction kinetics and thermodynamics it is possible that there will be some unreformed CH4 in the reformer gas if the reactor temperature is not sufficiently high. If thermodynamic equilibrium is assumed, a fuel reactor temperature in the order of 800ºC should be sufficient to achieve at least 99% conversion of CH4 at atmospheric pressure. At elevated pressure, somewhat higher temperature may be necessary due to less favourable thermodynamics.

1.3. Other studies done about Chemical Looping

1.3.1. Computational Fluid Dynamic studies (CFD) of CLC

The CFD-DEM model, or Computational Fluid Dynamics / Discrete Element Method model, is a process used to model or simulate systems combining fluids with solids or particles. In CFD-DEM, the motion of discrete solids or particles phase is obtained by the Discrete Element Method (DEM) which applies Newton's laws of motion to every particle, while the flow of continuum fluid is described by the local averaged Navier–Stokes equations that can be solved using the traditional Computational Fluid Dynamics (CFD) approach. The interactions between the fluid phase and solids phase is modeled by use of Newton's third law.

The results obtained from CFD have been compared with available experimental information. The transient CFD simulations provided a reasonable agreement with the reported experimental data for batch reactors using gaseous as well as solid fuels, and for a full circulating fluid bed CLC using gaseous fuels. The CFD models that were developed and validated using available experimental results have been applied for design evaluations of fuel reactor of CLC system utilizing char as fuel. It would be very desirable to utilize coal directly in the fuel reactor, which requires in situ gasification in either a moving or bubbling fluidized bed reactor. In such a design, H2O (and CO2) must be recycled from the product stream as the fluidizing medium, which allows in-bed heat transfer and mediates chemical reactions between the two solid feeds (carrier and fuel), and gasifies the coal char. The solid coal fuel must be heated by the recycled metal oxide, driving off moisture and volatile material, and the remaining char must then be gasified to provide complete fuel utilization. The gaseous products of these reactions must then contact the hot, oxidized carrier before leaving the bed to obtain complete conversion of the fuel to H2O and CO2. Further, the reduced carrier particles must be removed from the bed and returned as a pure stream to the air reactor for regeneration. It is critical that no unburned fuel, i.e., char, be returned with the spent carrier as this material will rapidly burn in the air reactor and the resulting CO2 will escape capture. Three designs have been developed and analyzed with CFD. Special attention is paid to Fe-based carriers (due to their low cost relative to other carriers), which is somewhat complicated due to the multiple oxidation states displayed by Fe. The non-linear interaction of factors such as multiphase hydrodynamics, heat transfer and chemical reaction is fully coupled in the numerical simulations allowing evaluation of design options for a full circulating CLC system using solid fuels.

1.3.2. Calcium and Iron Oxide Reactivity Studies for Chemical Looping

The hydration of calcium oxide (CaO) sorbent has been investigated as a reactivation method in the three step calcium looping process for pre and post combustion carbon dioxide (CO2) capture. The feasibility of the process concept was established using lab scale fixed bed reactor setup, and reactivation of sorbent was achieved with high temperature steam at 500°C over multiple cycles. Further development of the design and operation of a fluidized bed hydrator is reported upon, and fast fluidization regime was identified as the most suitable for a scalable steam hydrator design. Further, a screening study was conducted on multiple egg and sea shells as a renewable source of the CaO sorbent, and excellent reactivity towards CO2 is reported. A novel method for the simultaneous cleanup of CO2, SOx and NOx impurities from coal combustion flue gas is proposed based on the calcium looping process. Proof of concept experiments were performed and 90% CO2 and NO and 100% SO2 removal was demonstrated at 1 atm, 650°C fixed bed experiments, using the calcium sorbent and coal char. For pre- iii combustion application of the calcium looping process (CLP), the fate of sulfurous species is explored, which are formed as a byproduct of the coal to H2 plant with the CLP. The CaS formed in the carbonator at the operating conditions of about 600°C and 23 bar is found to be oxidized to CaSO4 at the calciner operating conditions of the CLP. Treatment options for the purge stream are discussed for the oxidation of unreacted CaS for the safe disposal and integration with the cement industry.

1.3.3. Mechanistic studies of chemical looping

In a laboratory reactor, it's subjected manganese-based materials to a periodically changing gas atmosphere, simulating a "chemical looping desulfurization" reactor. The "fuel reactor" gas contained H-2, CO, CH4 and H2S, similar as in the producer gas, and the "oxidizing reactor" contained diluted O-2. Mass spectrometry showed that most of the H2S is taken up by the sample in the "fuel reactor" part, while also some unwanted SO2 is generated in the "fuel reactor" part. Most of the sulfur is released in the oxidizing reactor. Simultaneous in situ X-ray absorption spectroscopy (XAS) of the Mn materials during different stages of the chemical looping desulfurization process showed that the initial Mn3O4 is transformed in the presence of H2S to MnS via a MnO intermediate in the fuel reactor. Oxygen from the reduction of Mn3O4 oxidizes some H2S to the undesired SO2 in the fuel reactor. Upon exposure to O-2, MnS is again oxidized to Mn3O4 via MnO, releasing SO2. The presence of CO and/or CH4 in the fuel reactor has no effect on this mechanism. Measuring the structure-performance relationship of gas cleaning materials with in situ methods will enable knowledge-based materials development for improved performance.

1.4. Thesis' study of the chemical looping

In that thesis it will be realized an analysis of a concrete chemical looping explained later. With this analysis the goal is to check if it's an efficient system. After the study through simulation, if it's efficient, it will be shown different useful applications to take advantage of chemical looping. Most of them are helpful to our planet's pollution.

1.5. Syngas Chemical Looping (study's chemical looping)

The SCL process can convert syngas with moderate levels of HCl, NH3, sulfur, and mercury; therefore, existing hot gas cleanup units (HGCU) will be adequate for raw syngas cleaning. The raw syngas exiting the HGCU will be introduced to the reducer, which is a moving bed of specially tailored iron oxide composite particles operated under a pressure similar to that of the syngas.

In this reactor, the syngas is completely converted into carbon dioxide and water while the iron oxide composite particles are reduced to a mixture of Fe and FeO under 750 - 900 °C:

$Fe_2O_3 + CO \rightarrow 2FeO + CO_2$
$FeO + CO \rightarrow Fe + CO_2$
$Fe_2O_3 + H_2 \rightarrow 2FeO + H_2O$
$FeO + H_2 \rightarrow Fe + H_2O$

Similar to the CLC processes, an exhaust stream with concentrated CO2 can be obtained from the reducer. The contaminants in the syngas will also exit the reducer with the CO2 stream without attaching to the particle. These contaminants can be

compressed and sequestered along with CO2 if allowed by regulation. As a result, the gas cleaning procedures are greatly simplified.

The Fe/FeO particles leaving the reducer are then introduced into the oxidizer which is operated at 500 – 750 °C. In the oxidizer, the reduced particles react with steam to produce a gas stream that contains solely H2 and unconverted steam. The steam can be easily condensed out to obtain a high purity H2 stream. The reactions involved in the oxidizer include:

$Fe + H_2O\ (g) \rightarrow FeO + H_2$
$3FeO + H_2O\ (g) \rightarrow Fe_3O_4 + H_2$

The steam used in the oxidizer is produced from the heat released from syngas cooling and reducer/oxidizer exhaust gas cooling. In the SCL process, the oxidizer is slightly exothermic while the reducer can either be slightly exothermic or slightly endothermic depending on the syngas composition. Therefore, both reducer and oxidizer are operated under the adiabatic conditions. Heat is provided to or removed from the reactors by the oxygen carrier particles and the exhaust gas. The Fe3O4 formed in the reducer reactor is regenerated to Fe2O3 in an entrained flow combustor which also transports solid particles discharged from the oxidizer to the reducer. A portion of the heat produced from the oxidation of Fe3O4 to Fe2O3 can be transferred to the reducer through the particles:

$4\ Fe_3O_4 + O_2 \rightarrow 6\ Fe_2O_3$

The high pressure, high temperature, spent air produced from the combustor can be used to drive a gas turbine - steam turbine combined cycle system to generate electricity for parasitic energy consumptions. In yet another configuration, a fraction or all of the reduced particles from the reducer can bypass the oxidizer and be introduced directly to the combustor if more heat or electricity is desired. Hence, both chemical-looping reforming and chemical-looping combustion concepts are applied in the SCL system, rendering it a versatile technology for H2 and electricity co-production.

Besides serving as a standalone hydrogen/electricity producer, the SCL process can be integrated into other processes to improve the overall energy conversion scheme. In this configuration, the SCL system converts the C1 – C4 products from the Fischer-Tropsch (FT) reactor into H2 and recycles it to the F-T reactor as feedstock, resulting in a 10% increase in the liquid fuel yield and a 19% reduction in CO2 emissions.

Oxygen carriers other than iron oxide such as NiO were also explored for hydrogen generation from syngas. The experiments carried out in a 20 mm I.D. fixed bed reactor, however, indicated that Fe is a more favorable choice than Ni. Svodoba (2007,2008) also examined, using thermodynamic principles, the feasibility of using Fe, Mn, Ni, Cr, and Co based particles for hydrogen production. They concluded that Fe – Fe3O4 is more suitable for chemical looping gasification compared to other particles; however, they further stated that Fe3O4 is more difficult to reduce based on a fluidized bed design.

2. Modelling of Study's Chemical Cooping cycle

The cycle to be used for the production of hydrogen and carbon dioxide capture from a syngas from gasification, consist of three reactors: the production of hydrogen, the oxidizer and the combustor. The solid chosen to be oxidized in the cycle is iron, besides stable and low cost.

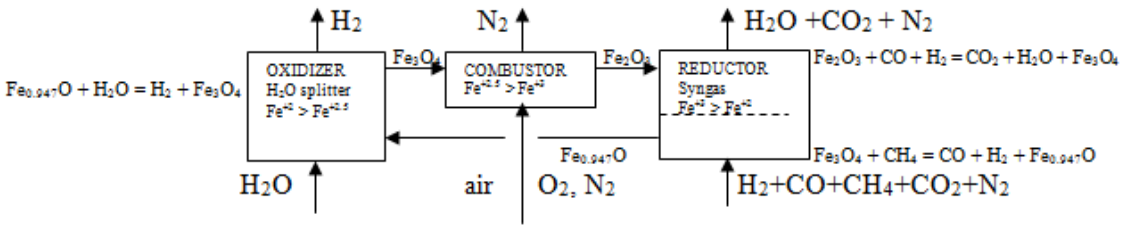

Figure 2.1. Study's Chemical Looping Scheme

That model will be iron-based composite oxygen carrier. That is currently being developed for the aforementioned chemical looping gasification process. The physical and chemical properties of the particles including compressive strength, attrition rate, reactivity and recyclability are tested. Reduction of the particles with syngas in an integral bed reactor is performed followed by oxidizing the reduced particles in the same reactor with steam and then air. More than 99.7% syngas is converted during the reduction step. During the regeneration step, hydrogen with an average purity of 99.8% is -IIIproduced. The results indicate that the particle is suitable for the chemical looping gasification processes.

Oxidizer

After being reduced in the reducer, a portion of the particles are introduced to the oxidizer. In the oxidizer, the reduced particles react with steam to produce a gas stream that contains solely H2 and unconverted steam. Once the steam is condensed out from the gas stream, an H2 stream of very high purity (> 99.95%) can be obtained. The reactions involved in the reducer reactor include:

$3.807\ Fe_{0.947}O + H_2O(g) = H_2(g) + 1.202\ Fe_3O_4$ $\quad \Delta H_{0°C} = -24.104$ kcal/mol H_2O

The steam used in the oxidizer is produced from the syngas cooling units and combustor. The oxidizer reactor operates at 30 atm and 500 – 750 ºC. By introducing the low temperature steam, the oxidizer is adjusted to be heat neutral. The heat released from the oxidation of the particles to Fe3O4 is used in the same reactor to heat the feed water/steam. The lower operation temperature of the oxidizer favors the steam to hydrogen conversion.

By using the syngas chemical looping process, CO2 is produced from a reactor different from where hydrogen is produced and hence, eliminating the energy consuming CO2 separation step

Combustor

Fe3O4 formed in the reducer is regenerated to Fe2O3 in a combustor. The combustor is a riser that conveys particles to the reducer with pressurized air. The combustor also serves as a heat generator since a significant amount of heat is produced during the combustion of Fe3O4 to Fe2O3:

$4\ Fe_3O_4 + O_2(g) = 6\ Fe_2O_3$ $\Delta H_{0°C} = -111.018$ kcal

The high pressure, high temperature gas produced from the combustor can be used for electricity generation to compensate the parasitic energy consumptions. In yet another configuration, part or all of the reduced particles from the reducer reactor can be directly sent to combustor without reacting with steam in the reducer reactor. By doing so, more heat would be available for electricity generation at the expense of decreased hydrogen production.

Reducer

The purified syngas is introduced to the reducer, which is a moving bed of iron oxide composite particles operated at 750 - 900 ºC and 30 atm. In this reactor, the syngas is completely converted to carbon dioxide and water while the iron oxide composite particles are reduced to FeO:

CH4(g) + 4.504 Fe2O3 = CO2(g) + 2 H2O(g) + 9.512 Fe0.947
ΔH0°C = +95.791 kcal

H2(g) + 1.126 Fe2O3 = H2O(g) + 2.378 Fe0.947O
ΔH0°C = +14.177 kcal

CO(g) + 1.126 Fe2O3 = CO2(g) + 2.378 Fe0.947O ΔH0°C = + 4.33 kcal

Global reaction:

$0.02CH_4(g) + 0.2H_2(g) + 0.18CO(g) + 0.51796\ Fe_2O_3 = 1.09388\ Fe_{0.947}O + 0.2CO_2(g) + 0.24\ H_2O(g)$

$\Delta H_{0°C} = +5.53062$ kcal

In the reducer, the syngas is nearly completely oxidized by the Fe2O3 composite particles. Thus, the exhaust gas from the reducer contains mainly CO2 and steam. Steam can be condensed out by extracting the heat from the high temperature exhaust gas, resulting in a concentrated high pressure CO2 stream that can be transported for sequestration.

The overall process is therefore shown schematically, with appropriate adjustment of the stoichiometric coefficients, such as:

Total cycle

0.02 CH4 + 0.0473 H2O + 0.0863 O2 + 0.18 CO = 0.0873H2 + 0.2 CO2 ΔH0°C = -10.98 kcal

The syngas charge is only used as a fuel and for the production of H2 using only its heat of combustion. The net production of hydrogen comes from the content of methane and CO present in the syngas feed.

The cycle seems to be able to fold in agreement with the evidence gathered so far, producing a current very concentrated in H2; free of sulfur compounds and possibly also a stream of N2.

3. Analysis of the three reactors

Before performing the looping the three different reactors will be tested to see if they complain the specifications needed.

Oxidizer

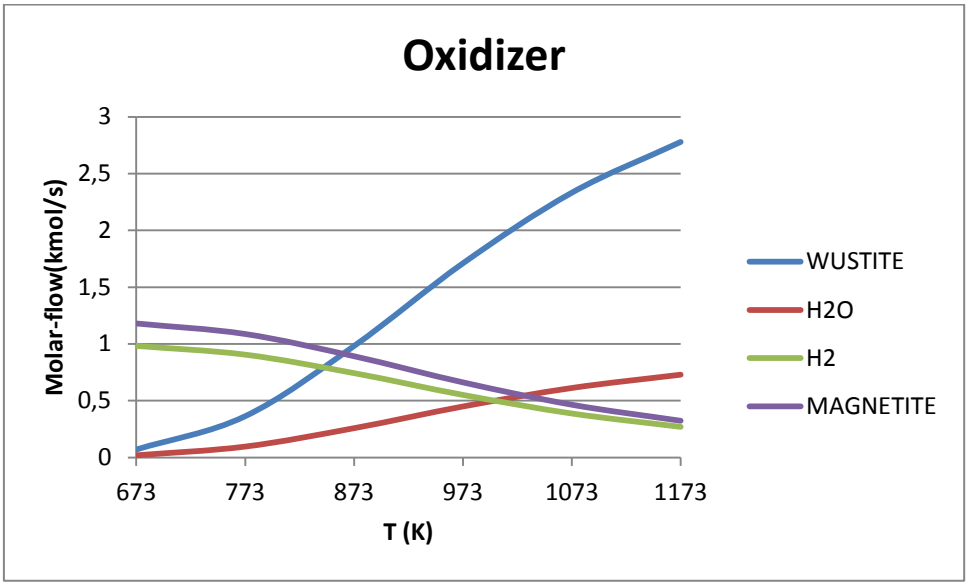

Figure 3.1. Molar flow-Temperature Graphic Oxidizer

As we can see, the ideal temperature to do the perfect reaction between wuestite and water steam is 400°C, but if it uses low temperatures like 300°C it's also better. If we continue elevating temperatures the reaction is practically inexistent.

Combustor

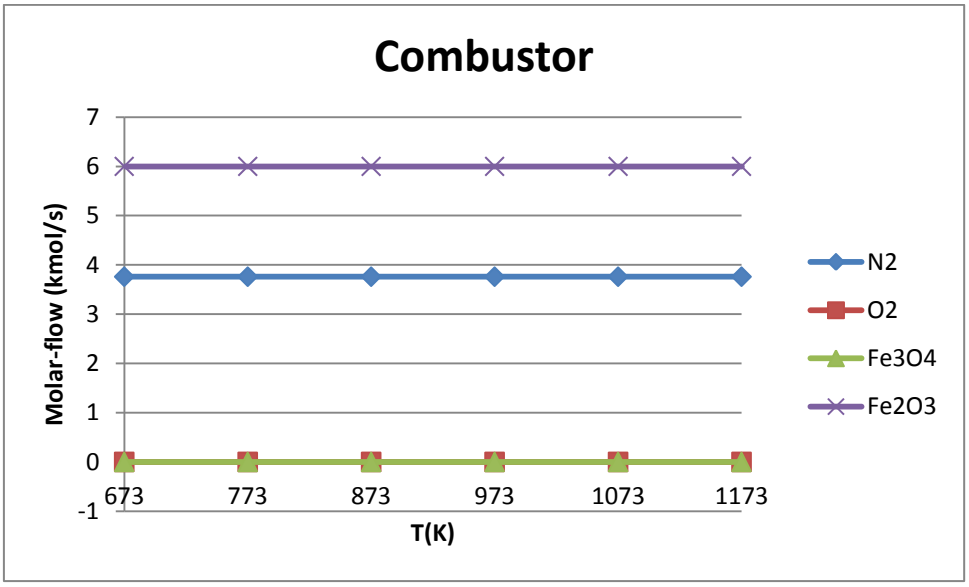

Figure 3.2. Molar flow-Temperature Graphic Combustor

It can be seen that it's an instantaneous combustion because from the beginning it makes the full conversion without intermediate steps related with the temperature. The conversion is what we expected without relationship with the temperature.

Reducer

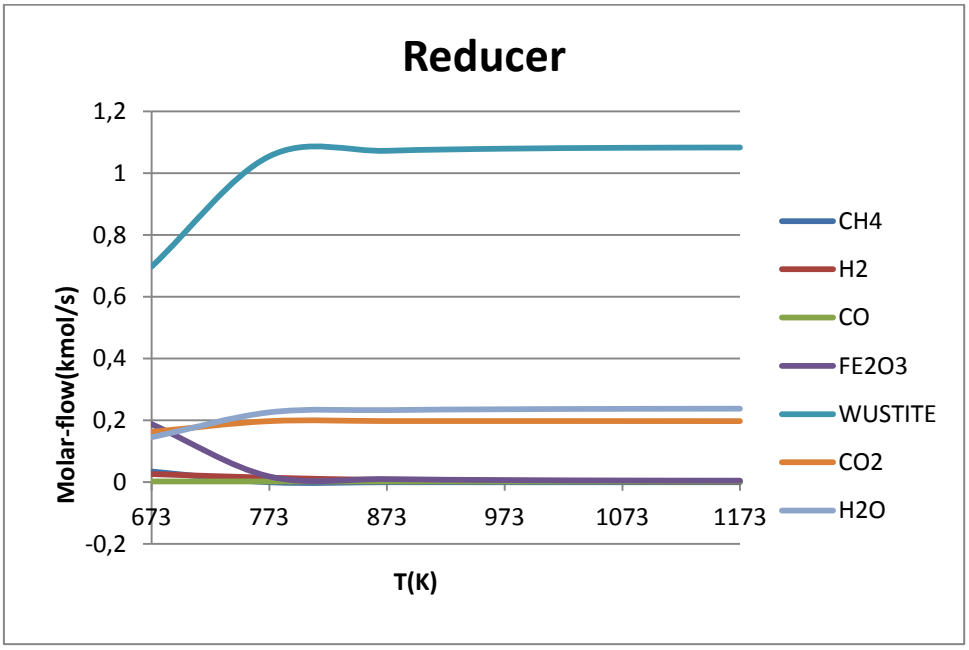

Figure 3.3. Molar flow-Temperature Graphic Reducer

The reactor as it can be seen realizes the perfect reaction at high temperatures, over 550°C.

4. Aspen plus technology

ASPEN PLUS™ is a software package designed to allow a user to build a process model and then simulate the model without tedious calculations.

ASPEN PLUS™ can be used for a wide variety of chemical engineering tasks. For example, it can execute tasks as simple as describing thermodynamic properties of an ethanol and water mixture, or as complex as predicting the steady-state behavior of a full-scale petrochemical plant.

Engineers are constantly being called upon to predict the behavior of systems. Chemical engineers in particular must be able to predict the actions of chemical species, a very difficult task. As chemical engineering students, when confronted with a large chemical system, you might ask, "Where do I even begin? Mass balances? Energy balances? Thermodynamic properties? Reaction Kinetics?" Over the past few years as a student you've learned about each of these crucial topics separately, however, "real world" situations will require an engineer to incorporate all of these areas.

To solve that problems appeared the idea of process model. A process model can be defined as an engineering system's "blue print." The process model is a complete layout of the engineering system including the following:

1. Flowsheet

The process model flowsheet maps out the entire system. The flowsheet shows one or more inlet streams entering into the system's first unit operation (i.e., heat exchanger, compressor, reactor, distillation column, etc.) and continues through the process, illustrating all intermediate unit operations and the interconnecting streams. The flowsheet also indicates all product streams. Each stream and unit operation is labeled and identified.

2. Chemical Components

The process model specifies all chemical components of the system from the necessary reactants and products, to steam and cooling water.

3. Operating Conditions

All unit operations in the process model are kept under particular operating conditions (i.e., temperature, pressure, size). These are usually at the discretion of the engineer, for it is the operating conditions of the process that affect the outcome of the system.

ASPEN PLUS™ allows you to create your own process model, starting with the flowsheet, then specifying the chemical components and operating conditions. It will take all of your specifications and, with a click of the mouse button, simulate the model. The process simulation is the action that executes all necessary calculations needed to solve the outcome of the system, hence predicting its behavior. When the calculations

are complete, ASPEN PLUS™ lists the results, stream by stream and unit by unit, so you can observe what happened to the chemical species of your process model.

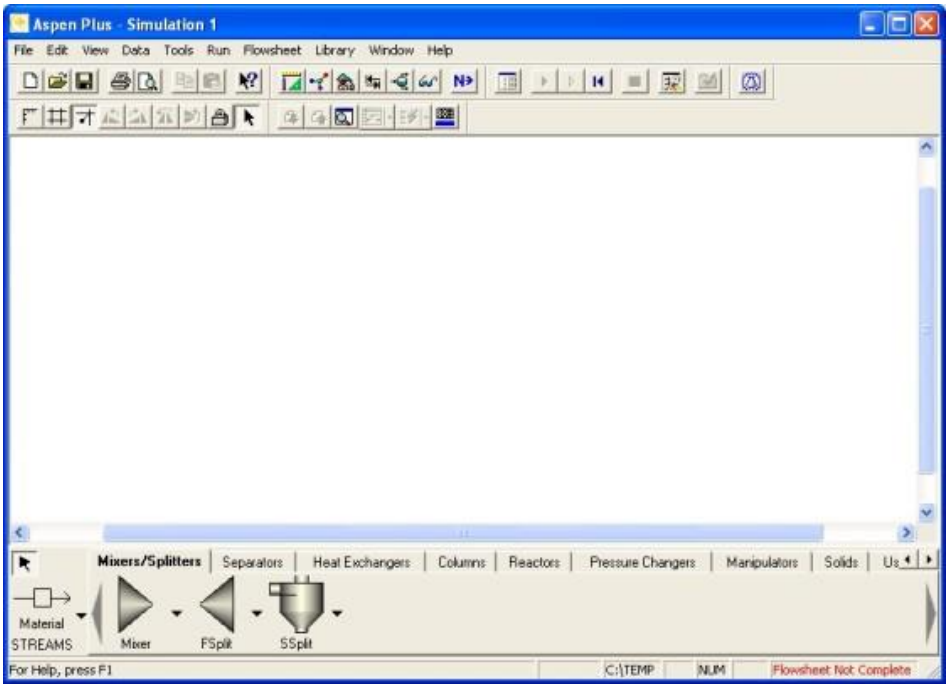

Figure 4.1. Aspen plus flowsheet

4.1. Elements used in the thesis cycle.

- Reactors

Model	Description	Purpose	Use
RSTOIC	Stoichiometric reactor	Stoichiometric reactor with specified reaction extent or conversion	When reaction kinetics are unknown or unimportant but stoichiometry and extent of reaction are known
RYIELD	Yield reactor	Reactor with specified yield	When stoichiometry and kinetics are unknown or unimportant but a yield distribution is known
REQUIL	Equilibrium reactor	Chemical and phase equilibrium by stoichiometric calculations	One- or two-phase chemical equilibrium and simultaneous phase equilibrium
RGIBBS	Equilibrium reactor (Gibbs energy minimization)	Chemical and phase equilibrium by Gibbs energy minimization	Chemical equilibrium. Simultaneous phase and chemical equilibrium. Phase equilibrium without chemical reactions. Phase equilibrium for vapor-liquid-solid systems and solid solutions.
RCSTR	Continuous stirred tank reactor	Continuous stirred tank reactor	Stirred tank reactors for vapor-liquid-solid systems with rate controlled and equilibrium reactions in any phase. Reaction kinetics are known.
RPLUG	Plug flow reactor	Plug flow reactor	Plug flow reactors for vapor-liquid-solid systems with rate controlled reactions in any phase. Reaction kinetics are known.
RBATCH	Batch reactor	Batch or semi-batch reactor	Batch and semi-batch reactors for vapor-liquid-solid systems with rate controlled reactions in any phase. Reaction kinetics are known.

Figure 4.2. Reactors

The reactor chosen has been RGIBBS due to its equilibrium, its capacity to work with solids and its Gibbs energy minimization.

- Separators

Model	Description	Purpose	Use
SEP	Component separator	Separate inlet stream components into outlet streams	Component separation operations (such as distillation and absorption), when the details of the separation are unknown or unimportant
SEP2	Two-outlet component separation	Separate inlet stream components into two outlet streams	Component separation operations (such as distillation and absorption), when the details of the separation are unknown or unimportant

Figure 4.3 Separators

The best option has been SEP because SEP 2 just separated liquid and vapor and in the thesis cycle there are also solids

5. Simulation of chemical looping cycle.

5.1. Simulation

After choosing the best elements to our cycle and check that the three reactors satisfy the desired requirements, the next step is to assemble the cycle.

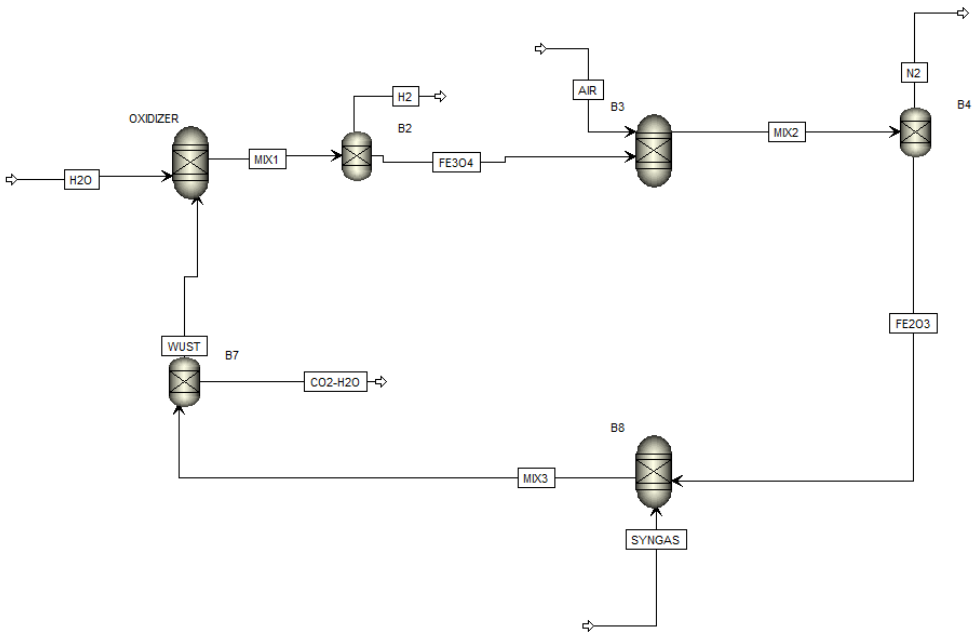

Figure 5.1. Study's Chemical Looping Cycle in Aspen Plus

Once the cycle is assembled, it's time to do the simulation to see if this cycle, chemical looping, is useful and helpful to complement thermodynamic plants more extensive and with different purposes.

After running the simulation without problems, results have to be checked and used to calculate the efficiency of the cycle.

		AIR	CO2-H2O	FE2O3	FE3O4	H2	H2O	MIX1	MIX2	MIX3	N2	SYNGAS	WUST
From			B7	B4	B2	B2		OXIDIZER	B3	B8	B4		B7
To		B3		B8	B3		OXIDIZER	B2	B4	B7		B8	OXIDIZER
Substream: MIXED													
Phase:		Vapor	Vapor	Solid	Solid	Vapor	Liquid	All	All	All	Vapor	Vapor	Solid
Component Mole Flow													
H2O	KMOL/SEC	0,0	,7298388	0,0	0,0	,0847562	1,000000	,0847562	0,0	,7298388	0,0	0,0	0,0
FE2O3	KMOL/SEC	0,0	0,0	1,800000	0,0	0,0	0,0	0,0	1,800000	0,0	0,0	0,0	0,0
FE0.947O	KMOL/SEC	0,0	0,0	0,0	0,0	0,0	0,0	0,0	0,0	3,484430	0,0	0,0	3,484430
FE3O4	KMOL/SEC	0,0	0,0	0,0	1,200000	0,0	0,0	1,200000	0,0	,1000815	0,0	0,0	,1000815
O2	KMOL/SEC	,3066000	0,0	0,0	0,0	0,0	0,0	0,0	6,60000E-3	2,0400E-17	6,60000E-3	0,0	0,0
CO2	KMOL/SEC	0,0	,4533746	0,0	0,0	0,0	0,0	0,0	0,0	,4533746	0,0	0,0	0,0
H2	KMOL/SEC	0,0	,2675552	0,0	0,0	,9152437	0,0	,9152437	0,0	,2675552	0,0	,3333333	0,0
CO	KMOL/SEC	0,0	,2119890	0,0	0,0	0,0	0,0	0,0	0,0	,2119890	0,0	,3333333	0,0
N2	KMOL/SEC	1,153400	0,0	0,0	0,0	0,0	0,0	0,0	1,153400	0,0	1,153400	0,0	0,0
CH4	KMOL/SEC	0,0	1,30301E-3	0,0	0,0	0,0	0,0	0,0	0,0	1,30301E-3	0,0	,3333333	0,0
Component Mole Fraction													
H2O		0,0	,4385891	0,0	0,0	,0847562	1,000000	,0385255	0,0	,1390547	0,0	0,0	0,0
FE2O3		0,0	0,0	1,000000	0,0	0,0	0,0	0,0	,6081081	0,0	0,0	0,0	0,0
FE0.947O		0,0	0,0	0,0	0,0	0,0	0,0	0,0	0,0	,6638815	0,0	0,0	,9720795
FE3O4		0,0	0,0	0,0	1,000000	0,0	0,0	,5454545	0,0	,0190683	0,0	0,0	,0279205
O2		,2100000	0,0	0,0	0,0	0,0	0,0	0,0	2,22973E-3	3,8869E-18	5,68966E-3	0,0	0,0
CO2		0,0	,2724508	0,0	0,0	0,0	0,0	0,0	0,0	,0863805	0,0	0,0	0,0
H2		0,0	,1607845	0,0	0,0	,9152437	0,0	,4160199	0,0	,0509767	0,0	,3333333	0,0
CO		0,0	,1273926	0,0	0,0	0,0	0,0	0,0	0,0	,0403898	0,0	,3333333	0,0
N2		,7900000	0,0	0,0	0,0	0,0	0,0	0,0	,3896622	0,0	,9943103	0,0	0,0
CH4		0,0	7,83033E-4	0,0	0,0	0,0	0,0	0,0	0,0	2,48261E-4	0,0	,3333333	0,0
Component Mass Flow													
H2O	KG/SEC	0,0	13,14825	0,0	0,0	1,526908	18,01528	1,526908	0,0	13,14825	0,0	0,0	0,0
FE2O3	KG/SEC	0,0	0,0	287,4460	0,0	0,0	0,0	0,0	287,4460	0,0	0,0	0,0	0,0
FE0.947O	KG/SEC	0,0	0,0	0,0	0,0	0,0	0,0	0,0	0,0	240,0302	0,0	0,0	240,0302
FE3O4	KG/SEC	0,0	0,0	0,0	277,8463	0,0	0,0	277,8463	0,0	23,17273	0,0	0,0	23,17273
O2	KG/SEC	9,810832	0,0	0,0	0,0	0,0	0,0	0,0	,2111921	6,5279E-16	,2111921	0,0	0,0
CO2	KG/SEC	0,0	19,95293	0,0	0,0	0,0	0,0	0,0	0,0	19,95293	0,0	0,0	0,0
H2	KG/SEC	0,0	,5393592	0,0	0,0	1,845021	0,0	1,845021	0,0	,5393592	0,0	,6719600	0,0
CO	KG/SEC	0,0	5,937898	0,0	0,0	0,0	0,0	0,0	0,0	5,937898	0,0	9,336800	0,0
N2	KG/SEC	32,31075	0,0	0,0	0,0	0,0	0,0	0,0	32,31075	0,0	32,31075	0,0	0,0
CH4	KG/SEC	0,0	,0209039	0,0	0,0	0,0	0,0	0,0	0,0	,0209039	0,0	5,347587	0,0
Mole Flow	KMOL/SEC	1,460000	1,664061	1,800000	1,200000	1,000000	1,000000	2,200000	2,960000	5,248572	1,160000	1,000000	3,584512
Mass Flow	KG/SEC	42,12158	39,59934	287,4460	277,8463	3,371930	18,01528	281,2182	319,9679	302,8023	32,52194	15,35635	263,2030
Average Molecular Weigh		28,85040	23,79681	159,6922	231,5386	3,371930	18,01528	127,8265	108,0973	57,69232	28,03616	15,35635	73,42784

Figure 5.2. Results of the simulation by steams.

As it's shown, the results are correct, complying what was expected. Coming up next efficiencies will be calculated.

$$\eta hyd\ theorical = \frac{HydrogenPowerOutput}{TotalPowerInput} = LHV_{H2}/\Delta H_{0°C} SyngasCH4 = (-242/-882)x100= 28\%$$

$$\eta hyd\ practical = \frac{HydrogenPowerOutput}{TotalPowerInput} = MWH2/MWsyngas= (3,37\ /15,35)x100= 22\%$$

5.2. Conclusions

Looking at the results the conclusion is that our cycle is efficient and can be useful. More H2 fuel could have been produced if Fe was generated in the reducer instead of FeO. Each Fe molecule has the ability to capture four times more oxygen than each FeO molecule. In this simulation, the reduction of Fe2O3 in the reducer only generates FeO. This output product composition is produced automatically in the RGIBBS reactor.

So if 100% Fe conversion could be achieved, four times more hydrogen could be produced, increasing the Hydrogen Generation Efficiency of the plant. Obviously, more heat would also be needed to start the desired reaction. In addition, this cycle will be more efficient joined as a complement to bigger cycles because off the complexity and accuracy of the thermal plant.

6. Applications of chemical looping technologies

Due to its efficiency and flexibility, chemical loopings are used in so many applications working with some fuels and gases. Here are the most important.

6.1. Hydrogen Storage and Onboard Hydrogen Production

Because hydrogen is an important clean energy source for the future, various hydrogen production technologies, including the chemical looping process, currently are being developed. The goal is to provide technically and economically feasible ways of generating hydrogen at a large scale. One key issue related to the application of hydrogen as a carbon - free, pollutant - free energy carrier is hydrogen storage. In particular, hydrogen has the potential to be the transportation fuel of the future, because it does not lead to CO 2 emissions that cause global warming. Unless hydrogen is used in a stationary energy conversion system, it has to be transferred to another site, generated in a distributed generation system or generated onboard a vehicle. However, economically storing or generating hydrogen onboard a vehicle at a high density (both volumetric and gravimetric) is a challenge. Thus, the development of high - capacity hydrogen storage materials has been one of the focal areas for energy research in recent years. The key factors to be considered for the development of hydrogen storage and/or onboard hydrogen generation systems are as follows: hydrogen capacity, cost, durability/operability, hydrogen charging/discharging rates, fuel quality, the environment, safety, and health. In what follows, a new onboard hydrogen generation system derived from chemical looping technology is introduced, as well as other, more extensively studied, hydrogen storage methods

6.1.1. Compressed Hydrogen Gas and Liquefied Hydrogen

Two of the simplest ways to store hydrogen are as a compressed gas and in liquefied form. Current commercially available high - pressure tanks are capable of storing hydrogen gas at 340 atm (5,000 psi) or 680 atm (10,000 psi). At 340 atm, the specific volume of hydrogen is 42 L/kg. Thus, for a tank containing 5 kg of hydrogen, this corresponds to a volume of 210 L, without accounting for the volume of the tank walls. Although the hydrogen is stored in pure form, when the weight of the tank is factored in (e.g., 86.3 kg for 4.7 kg of fuel at 204 atm), the gravimetric fuel capacity of high - pressure tanks is approximately 5 wt.%, which is significantly smaller than that of conventional liquid fuels.

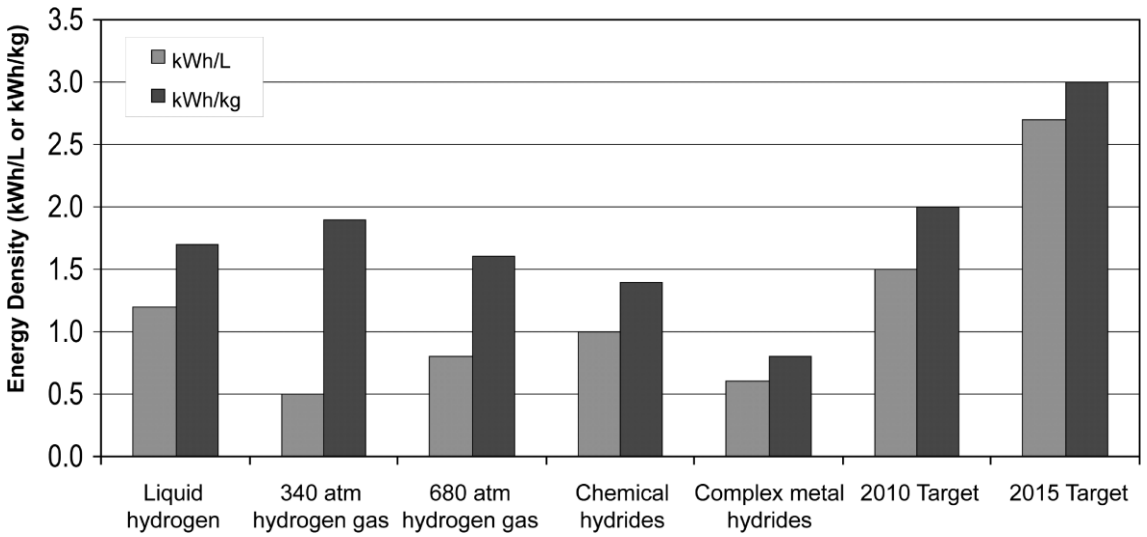

Figure 6.1. Gravimetric and volumetric energy densities of various hydrogen storage.

As shown in figure 6.1, the gravimetric and volumetric energy densities of compressed hydrogen gas at 340 atm and 680 atm still are substantially lower than the goals set by the DOE Freedom CAR Partnership. Considering the nonideal behavior of hydrogen gas at high pressure, the increase in pressure beyond 680 atm would not improve significantly the energy content of this storage option. For example, doubling the pressure from 680 atm to 1,360 atm would only increase the volumetric hydrogen gas density by 30%, whereas higher pressure requires a large increase in compression power. At 340 atm, it is estimated that 8.5% of the energy content of the hydrogen would be consumed in compression. Unlike conventional tanks for liquid fuels, which can be constructed in different shapes and dimensions to best use the available space, high - pressure tanks for hydrogen storage only can be cylindrical. This also limits the application of compressed gas as a hydrogen storage option. However, compressed hydrogen gas currently is a mature option for vehicular applications, and further research is ongoing for the purpose of cost reduction and lower tank weight design.

Another method of storing pure hydrogen is in the liquefied form. According to its phase diagram, hydrogen exists as a liquid at below − 253 ° C. Liquid hydrogen has a much higher density than compressed hydrogen with a specific volume of 14 L/kg, which significantly reduces the size of the onboard fuel tank. The major issues associated with liquefied hydrogen are the energy requirements for liquefaction and the dormancy period. The average energy consumption during liquefaction of hydrogen is 30% of the LHV (lower heating value of hydrogen), which is much greater than the energy for hydrogen compression to 340 – 680 atm. The dormancy period involves the gradual warming - up of hydrogen in the storage tank and the successive boil - off. Research has suggested that for a tank containing 4.6 kg of fuel, approximately 4% of the hydrogen will be boiled off per day. Thus, cryogenic tanks with advanced insulation are being developed to

overcome the dormancy issues. In particular, a high - pressure vessel, lined with aluminum and equipped with a composite outer wrap, a multilayer vacuum insulation, and an outer vacuum vessel, has been tested extensively and implemented in a demonstration vehicle. This vehicle can be fueled using either compressed hydrogen gas or liquid hydrogen depending on the desired driving distance.

A hybrid hydrogen tank is a relatively new idea consisting of a typical compressed hydrogen tank that is filled partially with low - temperature reversible hydrogen absorbing alloys. Typical reversible hydrides such as LaNi and FeTi can store hydrogen with volumetric densities of 6.7 – 7.7 L/kg at 100 ° C, which is several times greater than compressed hydrogen in terms of volumetric density. Because of its high volumetric energy density, this combined storage option can allow more compact hydrogen storage without sacrificing the advantages of a compressed hydrogen system. Compressed, liquefied, and hybrid tanks have the major advantage of instantaneously providing pure hydrogen at high rates, whereas other systems involving chemisorption or physisorption of hydrogen require a significant temperature swing to regenerate hydrogen on demand. Refueling also is relatively simple and fast because no chemical reactions are involved with the refilling of compressed and liquefied tanks, and the hydrogenation of the hydrides in hybrid tanks is considered to be rapid.

6.1.2. Metal Hydrides

Metal - hydride - based hydrogen storage is not a new technology and has been researched extensively during the past 30 years. Metal hydrides store hydrogen chemically in a crystalline structure that can pack more hydrogen into a given volume than liquid hydrogen. The reversible equilibrium reaction that involves hydrogen storage and regeneration can be written as follows:

$$MH_{n,solid} + Heat \leftrightarrow M_{solid} + (n/2)H_2 \qquad (1)$$

However, because hydrogen is very light and the metals usually are fairly heavy by comparison, the hydrogen storage per unit weight is not as high. Hydrides involving light elements such as Li, Be, B, N, Na, Mg, and Al generally have acceptable hydrogen storage per unit weight; but for binary hydrides of these elements, the binding energy is too strong to be practical. A high binding energy means that the hydride will only release hydrogen at high temperatures. For example, MgH_2 , one of the least stable binary hydrides among the light metals, has a theoretical hydrogen capacity of 7.6 wt.%, but its equilibrium hydrogen pressure only reaches 1 atm at about 300 ° C.

AlH_3 is a covalently bonded solid with 10.1 wt.% theoretical hydrogen storage that is actually thermodynamically unstable at room temperature. Because it is unstable at room temperature, it can release hydrogen at temperatures below 100 ° C. No currently known process could produce AlH_3 efficiently or on a large scale, and this recycling of Al to AlH_3 would have to be done offsite. Many other hydrides exhibit high hydrogen capacities and may have other favorable properties, but they have the same drawback as AlH_3 in that there is no known way to recharge the spent " fuel " efficiently or on a large scale. 19 However, current examples of a few known hydride reactions include hydrolysis of MgH_2 with water to produce Mg(OH) 2 and hydrogen, and catalytic hydrolysis of $NaBH_4$ (which can be stored as a 25%

solution in water) to produce aqueous $NaBO_2$ and hydrogen as shown in the following chemical reaction:

$$NaBH_4 + 2H_2O \rightarrow NaBO_2 + 4H_2 \quad (2)$$

These sorts of hydrides may still find specialty applications where economics are not the primary consideration, but they currently are not suitable for mobile applications. If, however, a simple and efficient process for regeneration of any of these compounds was developed, they could in fact meet the requirements for both volumetric and gravimetric energy density.

A hydride that both can release hydrogen and be regenerated under mild conditions is called a reversible hydride. These hydrides usually have equilibrium hydrogen pressures of 1 atm at mild temperatures ($\sim$ 0 – 60 ° C). With the proper catalysts, these hydrides can be generated from their metal alloys at room temperature and high pressure, and will release hydrogen at 1 – 2 atm at higher temperatures (still below 100 ° C). Early reversible metal hydrides include transition metal alloys such as $FeTiH_2$ and MNi_5H_6 , where M can be various transition metals. Interestingly enough, the latter compound already is used in Ni – MH rechargeable batteries found in many digital cameras and other electronics. Unfortunately, these alloys typically contain only 1 – 2 wt.% hydrogen and therefore, they are not suitable for mobile applications.

For a long time, sodium alanate ($NaAlH_4$) was considered to be in the same category as $NaBH_4$ and other irreversible hydrides despite having an equilibrium hydrogen pressure of 1 atm at $\sim$ 30 ° C. This changed in 1997 when Bogdanovic and Schwickardi reported that $NaAlH_4$ could be regenerated under relatively mild conditions when doped with certain transition metals. So far, the best results have been obtained using Ti as the dopant. Typical conditions for Ti - catalyzed rehydrogenation are 100 ° C and 100 atm. A balance must be achieved between the kinetics, which become more favorable as the temperature increases, and the thermodynamics, which become less favorable as the temperature increases. $NaAlH_4$ has a theoretical hydrogen storage capacity of 5.5 wt.%, and a reversible hydrogen storage of up to 5 wt.%. When the weight of the tank itself and the other components of the storage system are accounted for, the total system level capacity is expected to be only 2.5 wt.%. Current research tanks have a capacity of only 1 wt.%.

Other techniques that are worth noting, but are not yet well developed, include lithium imide/lithium amide systems and destabilized mixtures of multiple hydrides. Lithium imide can be hydrogenated to lithium amide with 6.5 wt.% reversible storage at around 250 ° C. Other than the relatively high temperature required, this system also has the drawback of producing small amounts of ammonia, which poison polymer electrolyte membrane (PEM) fuel cells even at trace levels. Destabilized mixtures of hydrides are formed by mixing a high - capacity, stable hydride with a compound that forms a stable intermediate with the hydride ' s dehydrogenated form. One such mixture is a blend of MgH_2 and LiBH 4 , which has been reported to have 9 wt.% reversible storage capacities, but this is only achieved at a high temperature and with slow kinetics. This particular blend achieves a high capacity, because both components have fairly high hydrogen capacities. Future research may produce more destabilized mixtures with more favorable kinetics and thermodynamics.

6.1.3. Bridged Metal - Organic Frameworks

The recent development of fundamentally new classes of nanoporous materials based on metal organic structures has been a significant development in the field of gas storage. Metal - organic frameworks (MOFs) are solids that consist of inorganic groups, usually $[ZnO_4]^{6+}$, bonded to linear aromatic carboxylates that form a robust and highly porous cubic framework. Of particular interest for hydrogen adsorption are the isoreticular MOFs, or IRMOFs, whose surface area and gas adsorption capacities are larger than other microporous materials such as zeolites and carbon nanotubes. MOFs are promising candidates for gas storage applications because they can be synthesized at high purity, with high crystallinity, potentially large quantities, and at low cost. Perhaps most importantly, MOFs can have an almost endless variety of structures and functional groups, leading to the possibility of rational design of sorbent materials tailored to specificapplications.

In recent years, IRMOFs by themselves have not produced spectacular results in terms of hydrogen adsorption at room temperature. For example, IRMOF - 1 (or MOF - 5) adsorbed hydrogen up to 4.5 wt.% at 78 K (− 195 ° C), but only adsorbed 1.0 wt.% at room temperature and 20 bar (2 MPa). 28 When MOFs are mixed with an active - carbon bridge, however, uptake at room temperature increased dramatically thanks to a phenomenon known as hydrogen spillover. Hydrogen spillover can be described as the dissociative chemisorption of hydrogen on one site, such as a metal particle, and the subsequent transportation of atomic hydrogen onto another substrate, usually carbon or alumina. In regard to the IRMOF structure, hydrogen rapidly dissociates and bonds to the metal/active carbon catalyst (Pt/AC), but slowly diffuses from the catalyst toward the MOF structure. It has been shown that surface diffusion of hydrogen atoms is the rate - determining step in hydrogen spillover. However, in the presence of carbon bridging, a secondary - spillover medium, the overall chemisorption process occurs faster. For example, Li and Yang have shown that the uptake of hydrogen onto carbon - bridged IRMOF - 8 at ambient conditions is eight times greater than that of pure IRMOF - 8 under the same conditions, and that the processes are completely reversible/rechargeable at room temperature.

Despite continued investigations and research on the kinetics of hydrogen spillover, the kinetics study of surface diffusion of hydrogen atoms under the ambient condition has not been reported. Moreover, the mechanistic details of hydrogen spillover still are not well understood. Thus, future investigation is needed to advance this hydrogen storage concept.

6.1.4. Carbon Nanotubes and Graphite Nanofibers

Carbon nanotubes (CNTs) generated considerable excitement when initial reports were published showing high storage capacities. Dillon et al. reported initial research on the storage potential of CNTs. They studied the adsorption of hydrogen on soot that contained 0.1 – 0.2 wt.% single - walled nanotubes (SWNTs) and extrapolated their data to determine a hydrogen storage capacity of 5 – 10 wt.%. Lee predicted a hydrogen storage capacity of up to 14 wt.% in SWNTs based on theoretical calculations. Multiwalled nanotube (MWNT) capacity was found to vary from 2.7 wt.% to 7.7 wt.%.

More recent studies have not been able to achieve the results predicted by Lee . Research conducted by Iqbal and Wang found hydrogen adsorption of 2.5 – 3.2 wt.% for SWNTs charged electrochemically. Reversible hydrogen storage of 1.5

wt.% was achieved with desorption taking place at 70 ° C. Dillon et al. conducted further research on hydrogen adsorption on MWNTs and found that although no hydrogen was adsorbed by clean MWNTs or iron nanoparticles under near - ambient conditions, MWNTs that contained significant quantities of iron nanoparticles were able to store 0.035 wt.% hydrogen. They concluded that the adsorption characteristics must result from an interaction between the MWNTs and the iron nanoparticles. Other studies have confirmed that the presence of metal nanoparticles is essential to hydrogen adsorption in both SWNTs and MWNTs. Most recent studies have found adsorption in the range of 1 – 4 wt.% for SWNTs and lower for MWNTs.

Graphite nanofibers (GNFs) are a nanostructured form of carbon consisting of layers of graphite formed into fibers. The individual layers of graphite may be parallel (tubular), perpendicular (platelet), or at an angle (herringbone) to the fiber axis. The length and diameter of individual GNFs can vary depending on many factors, but typical values include lengths of 50 μ m and diameters of 250 nm. GNFs can be formed by several processes, but the most common processes are thermal decomposition of hydrocarbons, typically acetylene, ethylene, or benzene, and catalytic graphitization of electrospun polymer fi bers, typically poly(vinylidene fluoride).

The fi rst research on the use of GNFs for hydrogen storage was published in 1998. Initial research done by Chambers achieved hydrogen adsorption varying from 11 wt.% for tubular GNFs to 67 wt.% for herringbone GNFs. Subsequent hydrogen desorption was reported to be as high as 58 wt.%. Adsorption took place at room temperature and at pressures ranging from 44 to 112 atm. Desorption took place at room temperature and atmospheric pressure. Ahn et al. conducted research on GNFs and other forms of activated carbon and found much lower storage capacities at room temperature and at 77 K (− 196 ° C). GNFs were found to adsorb approximately the same amount of hydrogen as other forms of activated carbon, with the best capacity being ∼ 1 wt.% at 77 K for GNFs. Fan et al. reported a hydrogen storage capacity of 10 – 13 wt.% for GNFs. More recent research done by Gupta found a hydrogen storage capacity of 17 wt.% for GNFs grown by thermal decomposition of acetylene on Pd sheets. Hong formed GNFs from electrospun poly(vinylidene fluoride) nanofibers and reported a storage capacity of 0.11 – 0.18 wt.%.

GNFs present a very attractive option for hydrogen storage due to their high storage capacity and their ability to both adsorb and desorb hydrogen at room temperature. However, the actual hydrogen storage capacity of these materials varies greatly, and the factors affecting this variance are not yet understood. All studies so far have focused on producing milligram or gram quantities of GNFs, but a commercial system for use in a typical automobile may require anywhere from 3 to 50 kg of GNF per vehicle. No process currently exists for the mass production of GNFs, and it is not known whether such a process could be economical. In addition, the ability of GNFs to withstand multiple hydrogenation/dehydrogenation cycles is not well understood. One study found that the capacity decreased by 30% after multiple cycles, whereas another study found the capacity actually increased over the first 10 cycles and remained constant thereafter. Although desorption of hydrogen from GNFs is very fast, adsorption takes hours to complete.

6.1.5. Onboard Hydrogen Production via Iron Based Materials

An onboard hydrogen production process such as one derived from the chemical looping strategy could be an option for the H_2 storage techniques discussed in the previous sections. When an iron based looping medium is used, this process allows the storage and production of hydrogen onboard a vehicle. This hydrogen storage system is based on the reaction of steam with Fe in order to produce hydrogen as described in the reaction:

$$3Fe+4H_2O \leftrightarrow Fe_3O_4 +4H_2 \qquad (3)$$

Thermodynamics dictates that for stoichiometric conversion of this reaction, steam must be made to react with Fe in a countercurrent fashion. This is easily achieved in a series of fixed bed reactors. TGA experiments show that a temperature above 400 ° C is sufficient to drive the reaction to completion. Although such an operating temperature is considered to be high relative to aforementioned metal hydride based hydrogen storage materials, and it requires a large amount of heat input for the hydrogen stored to be released, the exothermic nature of the steam iron reaction can potentially minimize the heat input for onboard hydrogen production using iron and steam. ASPEN simulations of Reaction show that if steam at 300 ° C is made to react with Fe at 25 ° C, the resultant heat of reaction will lead to an adiabatic temperature rise to 600 ° C. Hence, if a source of steam is available, Reaction can potentially be carried out without the need for extra heating devices. For the system to work, there needs to be a place to generate steam from water. A number of sources of heat may be utilized to achieve this.

Source 1: Hydrogen is produced at high temperatures, but for use in a PEM fuel cell the temperature of the hydrogen needs to be brought down to about 100 ° C. This heat may be used to generate steam.

Source 2: Additionally, more steam may be generated by using the heat from the oxidization of Fe_3O_4 to Fe_2O_3 in air.

$$2Fe_3O_4+1/2O_2 \rightarrow 3Fe_2O_3 \qquad (4)$$

Source 3: In case a hydrogen internal combustion engine (ICE) is used, heat can be absorbed from the engine using a suitable coolant (e.g., mineral oil) with a boiling point above 100 ° C to generate steam in a separate heat exchanger. If permitted by the specifications of the ICE, water may be directly injected to cool the engine resulting in steam production.

Source 4: The high - grade heat content of the exhaust from a H_2 ICE can be utilized to generate steam on board the vehicle.

Source 5: Use some of the Fe stored on board to react with air. This will allow for the combustion of Fe to Fe_2O_3, releasing a large amount of energy. For this purpose, a dedicated fixed bed can be put into the vehicle for heat generation. Water can be passed through this bed to capture the heat and generate steam.

$$4Fe+3O_2 \rightarrow 2Fe_2O_3 \qquad (5)$$

Source 6: The fuel cell device utilizing the hydrogen generates a large amount of heat. This heat may be integrated back to generate steam. A PEM fuel cell typically works in the 70 – 150 ° C range. The excess heat may be used to generate low grade steam.

Source 7: The hydrogen produced is put into a storage vessel. This vessel mainly provides hydrogen to the fuel cell, but part of the hydrogen stored may be routed back and combusted to generate heat for producing steam. For initial startup of the vehicle, a dedicated small hydrogen tank may be installed in the vehicle to switch on when the hydrogen storage tank does not have enough hydrogen pressure.

Source 8: The PEM fuel cell converts only about 90% of the hydrogen input. The remaining hydrogen may be combusted to provide heat for steam.

Source 9: Part of the electricity produced by the fuel cell and stored in the battery may be utilized to electrically heat the water using resistance heating to generate steam.

The water required for H_2 production may be recovered from the fuel cell exhaust in an air - cooled condenser that removes heat by convection into the ambient air when the vehicle is in motion. Greater than 90% of the water necessary is expected to be recovered in this manner. Additionally, in case it is desired, the exhaust may be routed through the air - conditioning system of the vehicle for further condensation, but this may impose an energy penalty on the system.
Once the Fe particles have been oxidized in the vehicle (to Fe 3 O 4 or Fe 2 O 3 as the case may be), they can be reduced back to Fe by utilizing a reaction with fuels:

$$[(2x+y/2-z)/3]Fe_2O_3+C_xH_yO_z \rightarrow xCO_2+(y/2)H_2O+[(4x+y-2z)/3]Fe \qquad (6)$$

The fuels may be a gaseous fuel like natural gas, producer gas, or syngas, a liquid fuel like gasoline, or a solid fuel like coal, or wood. In the case where Fe 3 O 4 is generated from the vehicle, Reaction (4) can be carried out first to convert it to Fe_2O_3 so that the CO_2 generation from Reaction (6) can be enhanced. This reaction will also help increase the temperature of the particles so that Reaction (6) can readily proceed.

Reaction (6) will likely need to be conducted outside the vehicle at a central fuel station. Such a centralized station may be built outside a city where the spent particles can be regenerated and distributed to retail outlets.

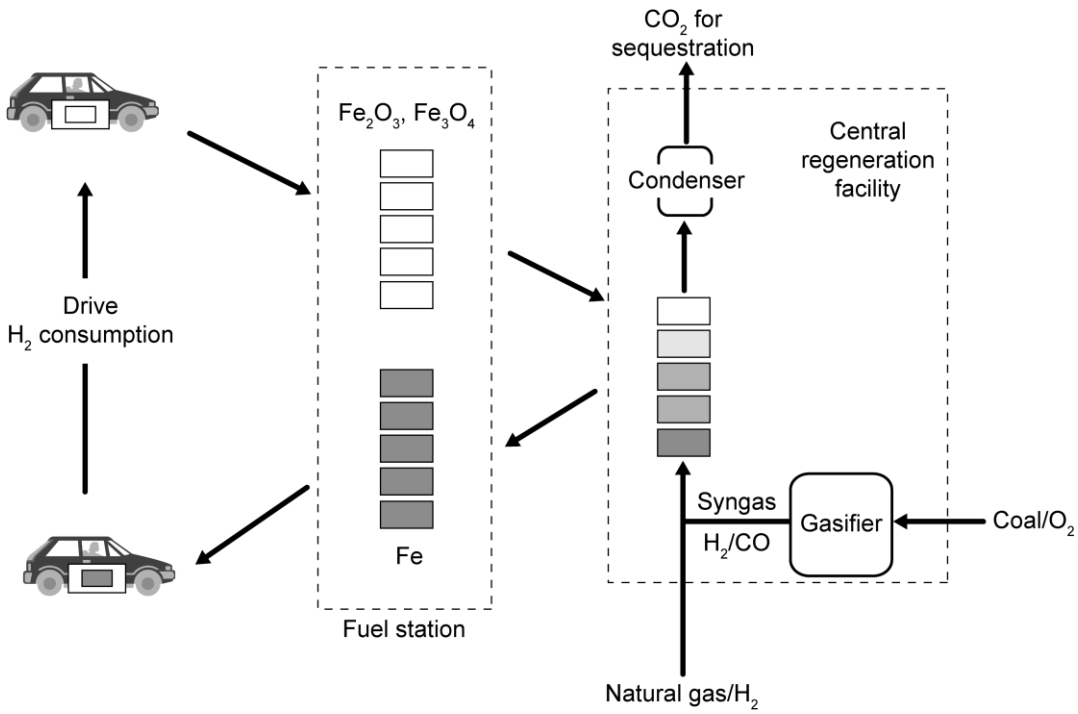

Figure 6.2. Overall scheme of using Fe modules to produce hydrogen on a vehicle.

Figure 6.2 shows the overall scheme for using iron to produce hydrogen on a vehicle. The design of the particle regeneration rectors given in the figure involves the flow of reactive fuel countercurrent to the flow of the spent particles. The regenerated iron particles exit from the reactor and can be used for producing hydrogen on board the vehicle.

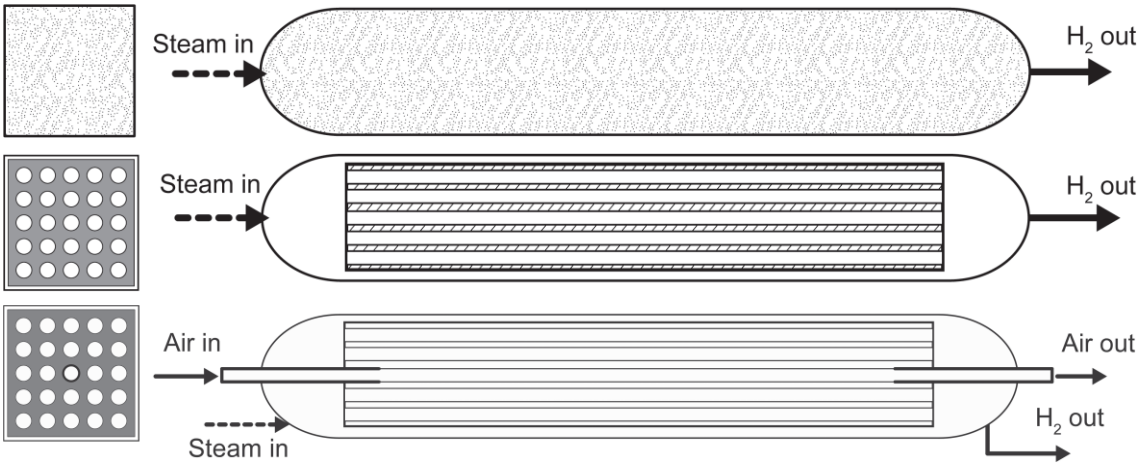

Figure 6.3. Designs for reactors with Fe containing media: packed bed of small pellets; monolithic bed with straight channels for steam; and monolithic bed with channels for steam and air.

The hydrogen generation can be carried out in a packed bed reactor or a monolithic bed reactor as shown in Figure 6.3. The steam can pass through the reactors at high temperatures and react with iron to form hydrogen. For a packed bed reactor shown in Figure 6.3 (first), the particle formulation can be cast into small pellets of 1 – 5 mm in size. These pellets can be randomly packed into a metallic vessel to establish a packed bed. It is desired that the metallic vessel is of a rectangular cross section for close packing in a module, though circular cross section can also be used. The designs for the monolithic bed reactors are shown in Figures 6.3 (second) and 6.3 (third). The monoliths in the design are of ceramic structures with channels/holes present over the length of the structure. This structure allows the packing of iron particles in a confined space. With suitable design on end caps, it is possible to route fluids through different channels. It also allows air to pass through some channels, while steam flows through other channels, as shown in Figure 6.3 (third). This functionality could provide the heat, released from Reactions (4) and (5), for generation of steam used for its reaction with iron. In all designs, refractory lining or vacuum jacket could be used to prevent heat losses from the reactors. It is noted that in module design, iron can also be embedded in the ceramic channel wall materials. In this case, both the reduction and regeneration reactions take place directly on the module.

An important aspect of the iron particle regeneration process is that the gaseous products from Reaction (6) will mainly be steam and CO_2. After condensation of steam, the CO_2 rich stream can be easily separated and sequestered using the same carbon sequestration techniques intended for stationary power plants. Hence, the process can potentially save the cost for CO_2 capture. Further, since no CO_2 is emitted from the vehicle, the overall scheme provides a viable method for CO_2 emission control when a suitable CO_2 sequestration technique is available.

A number of such reactors may be required for generating an adequate quantity of H_2 for use in a transportation vehicle. Also, if the reactors are connected in series, the H_2 purities obtained can be very high. Such a series reactor assembly forms the key component of a module that can be used for onboard hydrogen production applications.

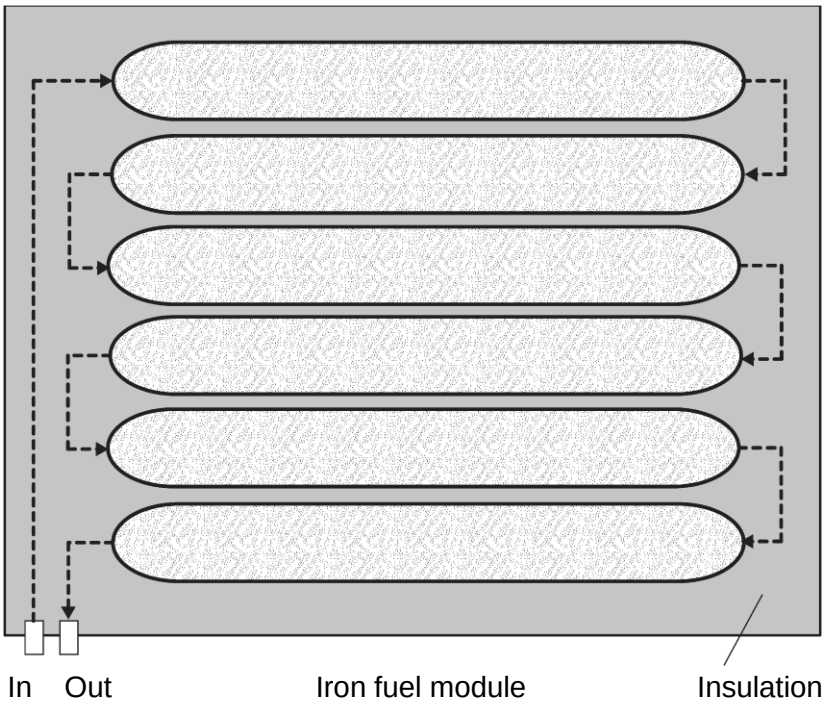

Figure 6.4. H_2 production module using a series of fixed - bed reactors.

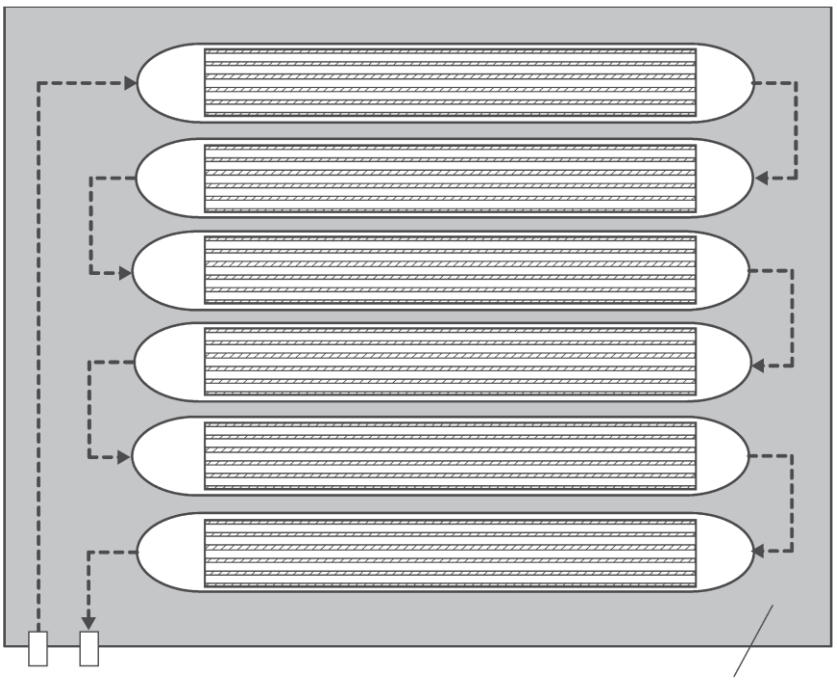

In Out Iron fuel module Insulation

Figure 6.5. H_2 production module using a series of monolithic - bed reactors.

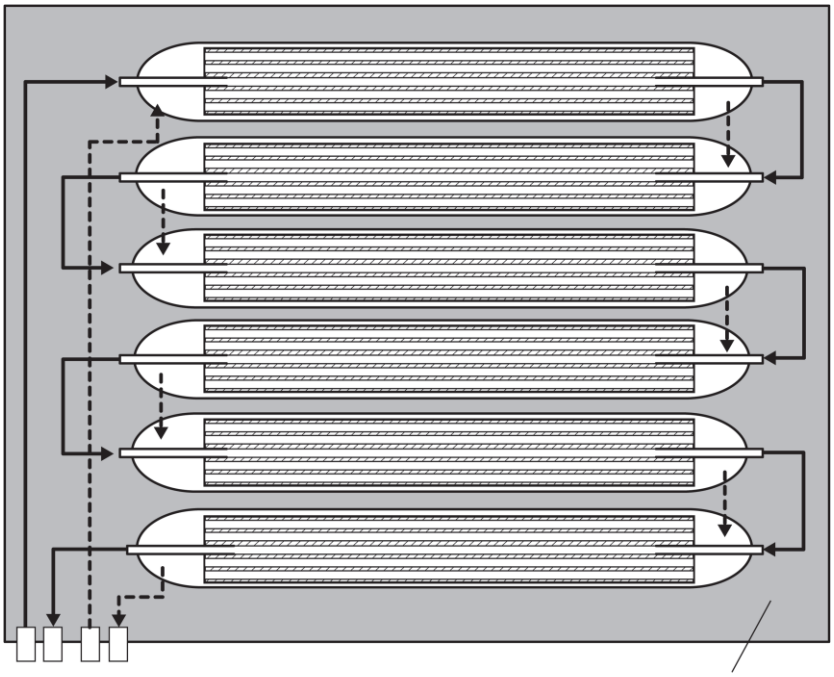

In Out In Out Iron fuel model Insulation
Air Steam

Figure 6.6. H_2 production module using a series of monolithic - bed reactors with air injection to provide heat for steam formation.

Figures 6.4, 6.5 and 6.6 present some configurations for the modules made up of the reactors shown in Figure 6.3 . The reactors are connected using metallic tubing welded to the end caps. The reactor assembly is enclosed in a suitable metallic box/container with insulation to prevent loss of heat to the surroundings. Depending on the heat integration scheme, the number of fluid inlet and outlet points may be varied. In the simplest scheme, as shown in Figures 6.4 and 6.5, there are only one inlet (steam) point and one outlet (H_2) point. The fluid flow lines can be connected to or disconnected from the module using quick - connect couplings. The module can easily be loaded to or unloaded from a transportation vehicle.

Such modules may be directly purchased from a retail store. These may also be sold through “ Iron Stations ” or the “ Fuel Station, ” the future equivalent of gas stations, as shown in Figure 6.2 . It is note that even though Reaction (3) takes place at a temperature above 400 ° C, within the reactors, only the region proximate to where the reaction front is developed will be hot.

System Integration Onboard a Transportation Vehicle

A number of scenarios can be considered in regard to the integration of the Fe modules with other components in a transportation vehicle. Two most relevant scenarios are presented in the following. Other scenarios may be conceived by combining the concepts discussed in these scenarios.

Scenario 1: Use of H 2 ICE Heat to Produce Steam. The heat generated, but not utilized for shaft work in a H_2 ICE, is enough to generate the steam required to produce hydrogen. This heat is taken away from the engine using the coolant and the exhaust, and may be recovered to produce steam.

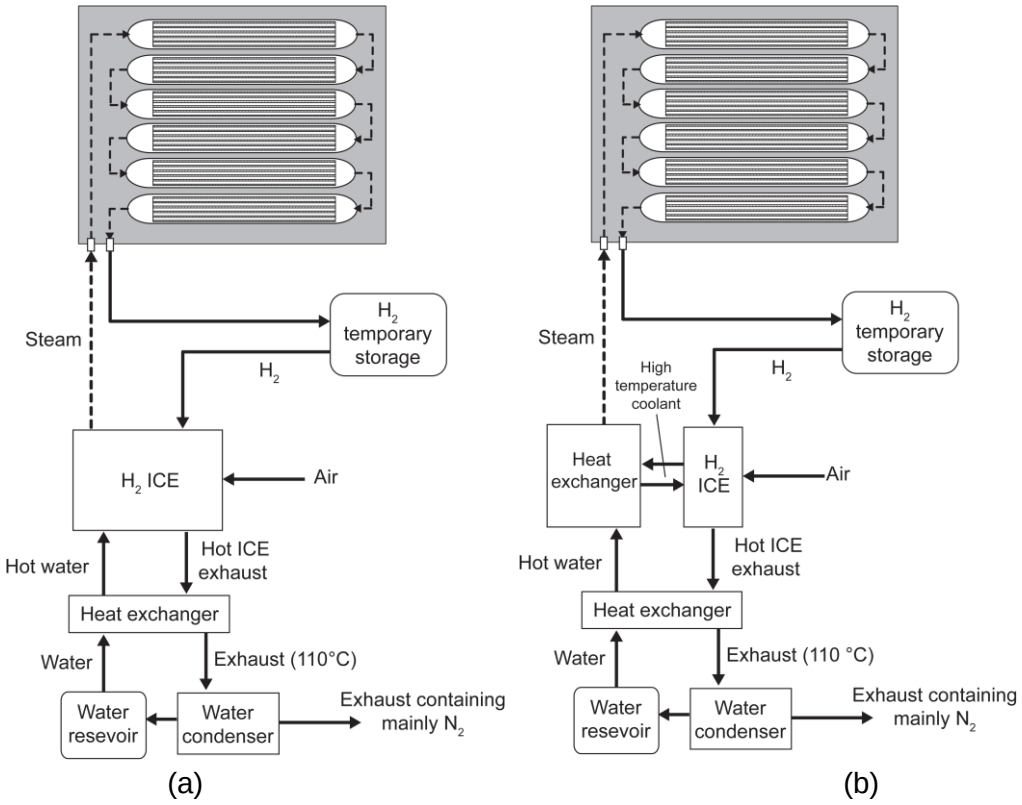

Figure 6.7. System integration for use of Fe module with a H_2 ICE using, (a) water to cool the ICE and (b) a high - temperature coolant to cool the ICE.

Figure 6.7 shows such integration. A minimal amount of water makeup may be required if the exhaust water can be recovered using a condenser. Such a condenser may be cooled using the water reservoir or using convective heat transfer to air. Once started, the system is self-sustaining on heat until the time all of the Fe in the module is consumed.

Scenario 2: Use of Oxidation Reactions of Fe and Fe_3O_4 to Provide for Steam Formation Heat. This scenario does not require integration with the fuel cell or the H_2 ICE. Hence, this scenario can be used to provide hydrogen with stand - alone Fe module usage.

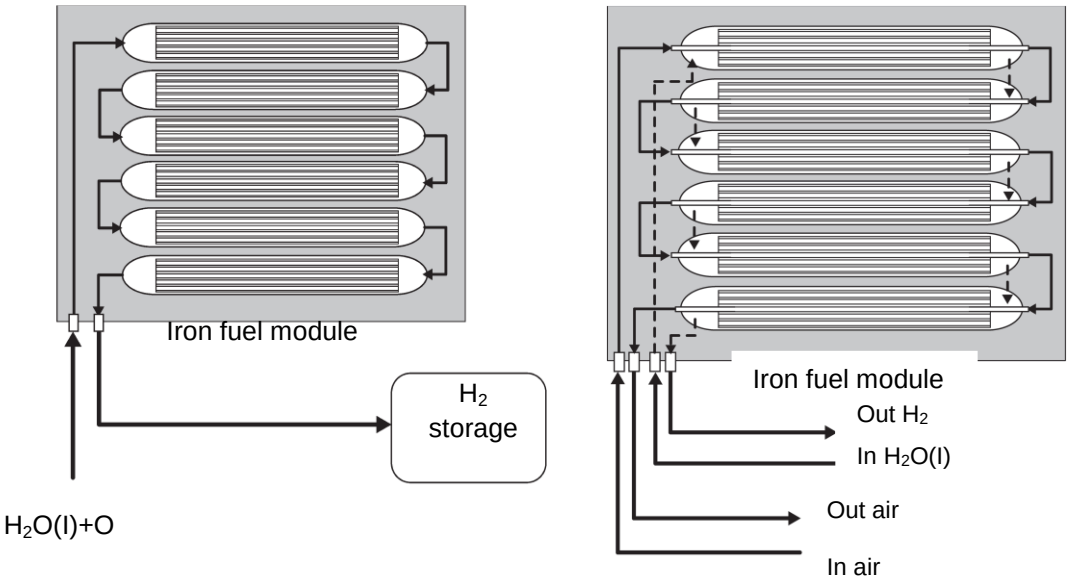
Iron fuel module
H_2 storage
$H_2O(l)$+O
Iron fuel module
Out H_2
In $H_2O(l)$
Out air
In air

(a) (b)

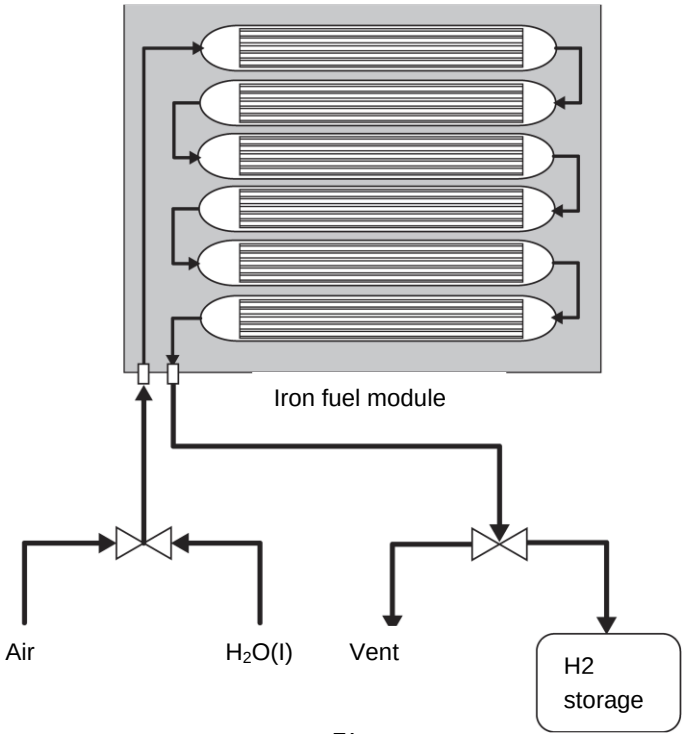
Iron fuel module
Air
$H_2O(l)$
Vent
H2 storage

(c)

Figure 6.8. Hydrogen production from a stand - alone Fe module.

Air is supplied along with steam into the Fe modules, as shown in Figure 6.8. This air then oxidizes the Fe/Fe_3O_4 to Fe_2O_3, releasing heat that takes the unreacted Fe particles to reaction temperatures of higher than 400 ° C. The configuration shown in Figure 6.8 (c) involves first sending air through one packed reactor. Water is then added and being converted to steam. Steam reacts with Fe in the remaining reactors to produce hydrogen. For this operation, one reactor bed in the Fe to Fe_2O_3 oxidation mode with air is required to produce hydrogen from five Fe reactors.

Meeting DOE Targets

The energy density of the Fe composite particles, when fully reduced, is calculated to be up to 1.52 kWh/L or 1.17 kWh/kg of the particles. It is comparable to the DOE 2010 target of 1.5 kWh/L for the volumetric energy density. Since the raw material for producing the composite particle is inexpensive and its synthesis procedure is not elaborate, the cost for this on - board hydrogen production option has the potential to meet the DOE target of $2/kWh set for 2015. The potential challenges to this option, however, include relatively high reaction temperatures and delicate heat integration requirement.

6.2. Carbonation-Calcination Reaction (CCR). Carbon Dioxide Capture

Carbon dioxide capture is the most expensive step of the overall threefold carbon management step, which consists of separation, transportation, and sequestration. The ongoing research and development (R & D) on carbon management includes mapping the strategy for CO_2 separation. Such strategies include improving the energy - intensive low - temperature amine scrubbing process, demonstrating the chilled ammonia process, developing further oxycombustion technology (in which high - purity oxygen is used for combustion), and employing reactive CO_2 separation using dry, solid sorbents such as limestone, potassium carbonates, lithium silicates, and sodium carbonates, which yield a sequestration - ready CO_2 gas stream upon decomposition. Other processes being investigated include low - temperature pressure swing adsorption processes using hydrotalcite. Thus, cost - effective carbon - capture technologies play an important role in CO_2 mitigation for current plant operation. In a typical flue gas stream (dry basis) generated from coal combustion power plants, the concentration of CO_2 is low, representing approximately 15% of the flue gas stream. Low CO_2 partial pressures, combined with the extremely high flue gas generation rate, make CO_2 capture from PC power plants an energy - intensive step. An ideal CO_2 capture technology would incorporate effective process integration schemes to minimize the parasitic energy required for CO_2 separation.

One process alternative uses a calcium - based solid sorbent at a high temperature to capture CO_2 and SO_2 simultaneously. The CCR Process, which is an outgrowth of two other processes developed at The Ohio State University: the Ohio State Carbonation Ash Reactivation (OSCAR) Process and the Calcium - Based Reaction Separation for CO_2 (CaRS – CO_2) Process, uses calcium oxide to react with the CO_2 and SO_2 present in the flue gas stream at a high temperature (450 – 750 ° C). Similar to the Calcium Looping Process for hydrogen production, the calcium oxide can be derived from multiple sources including hydrated lime, natural limestone, or reengineered calcium carbonate, such as Precipitated Calcium Carbonate (PCC).

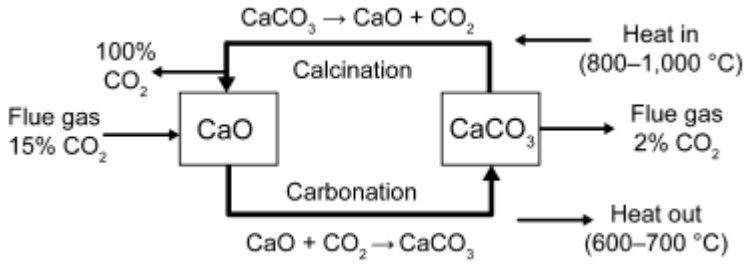

Figure 6.9. CO2 Capturing and Separation Scheme

The concept of capturing and separating CO2 from flue gas using limestone - based sorbents is depicted in Figure 6.9 . The flue gas comes into contact with calcium oxide (CaO), which reacts with the CO_2 and SO_2 in the flue gas to form calcium carbonate ($CaCO_3$) and calcium sulfate ($CaSO_4$). During the carbonation and sulfation reactions, which typically take place between 600 ° C and 700 ° C, heat is released. The reacted sorbent is regenerated in a separate step by decomposing $CaCO_3$ at higher temperatures (greater than 850°C) to yield CaO and CO_2 . The thermal stability of calcium sulfate ensures that it does not decompose and remains as calcium sulfate. By calcining the sorbent in a proper environment, the degeneration of the reactivity of regenerated calcium sorbent can be minimized while yielding a pure or concentrated gas stream of CO_2 that can be compressed and transported for sequestration. The process thus can take a flue gas that contains typically 10 – 15% CO_2 and convert it into a nearly pure (> 90%) CO_2 stream.

Next reactions summarize the basic chemistry involved in the process:

Carbonation: $CaO(s)+CO_2(g)\rightarrow CaCO_3(s)$ $\Delta H = -178$ KJ/mol

Calcination: $CaCO_3(s)\rightarrow CaO(s)+CO_2(g)$ $\Delta H = +178$ KJ/mol

As shown here, the carbonation process is exothermic, whereas calcination requires heat input. The heat integration is thus essential, in that the heat released at temperatures of 600 – 700 ° C during the carbonation process needs to be recovered and used, whereas additional heat energy is necessary for the calcination reaction.

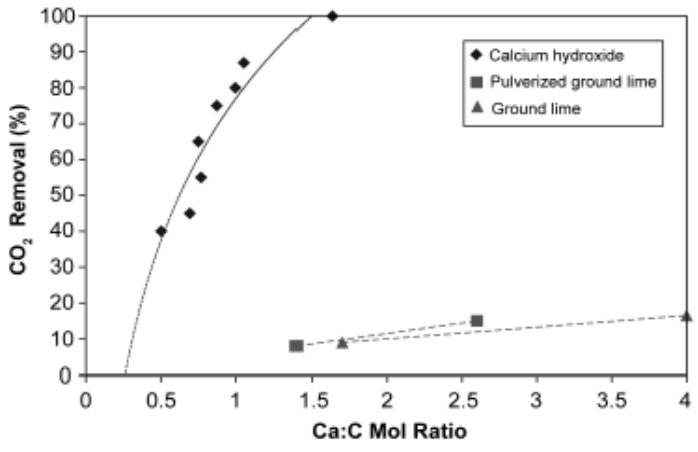

Figure 6.10. Effect of Ca:C molar ratio on the CO 2 removal efficiency for three Ca -based sorbents.

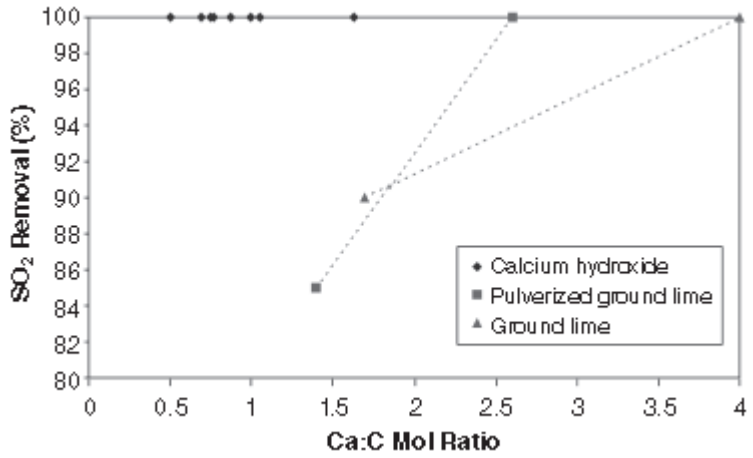

Figure 6.11. Effect of Ca:C molar ratio on the SO_2 removal efficiency for three Ca - based sorbents.

Sorbent reactivity has a significant effect on the CO_2 removal efficiency. Therefore, the type of sorbent has a considerable effect on the overall CO_2 removal, as shown in Figure 6.10 . The data were obtained from an entrained bed reactor using a flue gas stream generated by coal combustion at 9 kg/h, which will be illustrated in further detail later. Clearly, the superior performance of calcium hydroxide is evident as compared with other inexpensive calcium - based sorbents in removing CO_2. As mentioned, sulfur dioxide also is removed simultaneously from the flue gas stream. Figure 6.11 shows the effect of the Ca:C molar ratio on SO2 removal. Even at low Ca:C molar ratios, virtually all the SO_2 is captured effectively and removed by the calcium hydroxide sorbent. This is a result of the significantly lower concentration of SO_2 as compared with CO_2 in the flue gas stream. A 1:1 Ca:C molar ratio corresponds to an 80:1 Ca:S molar ratio.

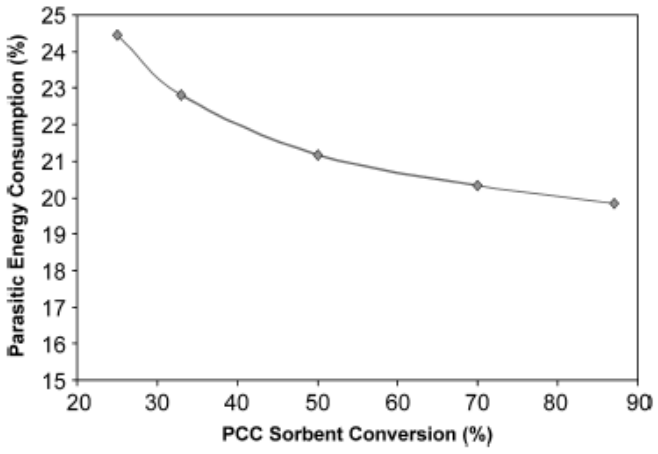

Figure 6.12. Relationship between the parasitic energy consumption and PCC sorbent molar conversion efficiency.

Parasitic energy consumption is related strongly to the sorbent conversion efficiency in the looping operation. Figure 6.12 shows such a relationship for PCC, which is a reengineered calcium carbonate sorbent with a reactivity slightly higher than the hydrate - based sorbent. It is shown that the parasitic energy consumption for the CCR Process can be significantly lower than that for such low - temperature CO_2 capture processes as the MEA process, as discussed earlier, when the sorbent conversion efficiency reaches 30% – 70%.

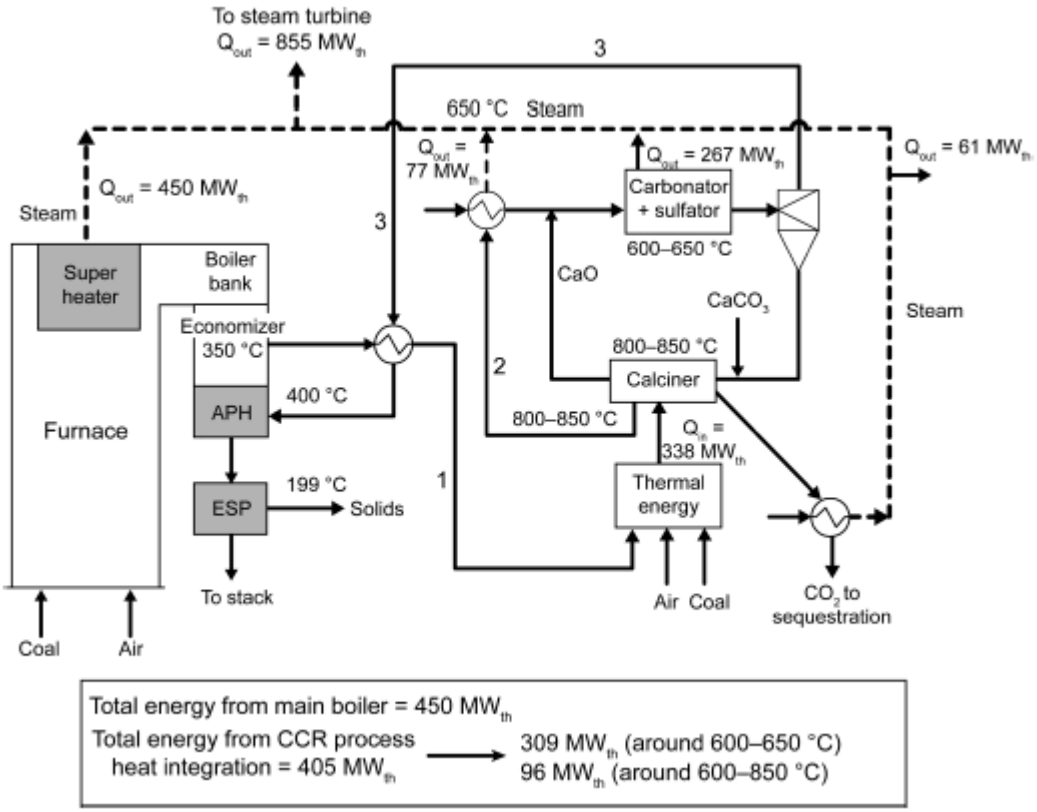

Figure 6.13. Conceptual schematic of Carbonation – Calcination Reaction (CCR) Process integration for a 300 - MWe (900 - MWth) coal - fi red power plant depicting heat integration strategies.

Figure 6.13 delineates the heat integration strategies for retrofitting the CCR Process to an existing boiler for 90% CO_2 capture without significant modifications to the coal - based power plant. The flue gas that leaves the economizer of the boiler is routed to the CCR Process system for CO_2 capture. This flue gas from the economizer (stream 1) is combined with the flue gas used to generate the heat required to operate the indirectly fired calciner. Heat is extracted from the total flue gas mixture (stream 2), which contains all the CO_2 emitted by the entire plant, before being sent into the carbonator system for carbonation and sulfation. CO_2 is removed in the carbonator system, and the CO_2 free flue gas (stream 3), which is at ~ 650 ° C, is cooled before it is sent into the air preheater followed by the electrostatic precipitator (ESP). In the carbonator, SO_2 and traces of heavy metals including selenium and arsenic also are removed, rendering the CCR Process a multipollutant control process. The spent sorbent from the carbonation system is sent to the calciner to regenerate the calcium oxide (CaO) sorbent for

subsequent cycles while yielding a pure CO_2 stream. The sulfated sorbent and fly ash are removed from the system by means of a purge stream, whereas the makeup fresh sorbent is introduced into the system. The amount of solids removed through the purge stream is entirely dependent on the concentration of fly ash and calcium sulfate in the solids stream, which are both coal dependent. The heat of carbonation can be as high as one third of the total thermal capacity of a power plant. In the CCR Process, steam is generated using high - quality heat available from three different sources: (a) the carbonation system (450 – 750 ° C), (b) the hot flue gas generated for calciner operation (greater than 850 ° C), and (c) a pure CO_2 stream from the calciner (greater than 850 ° C). This steam can be used in a secondary steam turbine system for additional electricity generation or in the existing plant steam cycle by offsetting the boiler load and in driving various feed water pumps in the plant. Figure 6.13 indicates that the heat balance from each unit in the process gives rise to the thermal energy produced for steam generation of 855 MWth , reflecting a loss of 45 MWth or 5% in the CCR Process. This small energy loss is for an ideal system without CO_2 compression. With the inclusion of the energy requirement for CO_2 compression to 150 atm (2,200 psi) and other process heat losses, the parasitic energy consumption increases from 5% to 20% – 24%, as given in Figure 6.12 .

Figure 6.14. Subpilotscale - CCR Process facility located at The Ohio State University.

The CCR Process is being demonstrated in a 120 - KWth subpilot plant, as shown in Figure 6.14 , located at OSU. The OSU system consists of a 9 - kg/h coal - fired stoker furnace, a rotary calciner, sorbent and ash injection systems, baghouse, fans, particulate control devices, data acquisition and control systems, and associated instrumentation. Because most residual ash drops out from the stoker furnace, makeup fly ash can be injected using a screw feeder to simulate gas from a typical pulverized coal - fired boiler. The gas that exits the furnace is first cooled to the required carbonation temperature of 600 – 700 ° C prior to the sorbent injection point. Sorbent then is injected to remove CO_2 and SO_2 reactively from the flue gas. The reacted/spent sorbent then is separated from the flue gas and sent to the calciner for regeneration. The CO_2 - depleted flue gas is cooled to approximately 50 ° C by aspirating ambient air into the gas stream. The cooled flue gas is then sent into a baghouse where the remaining sorbent and fly ash are separated. The calciner regenerates the spent sorbent, which is then conveyed back into the process for a subsequent CO_2 capture cycle. A screw feeder system is used for sorbent delivery.

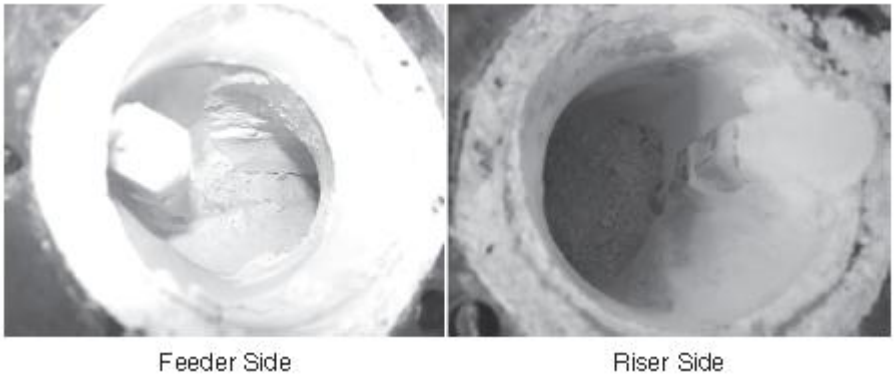

Figure 6.15. Internal view of the U - bend section of the subpilot - scale facility (given in Figure 6.14) after one week of operation.

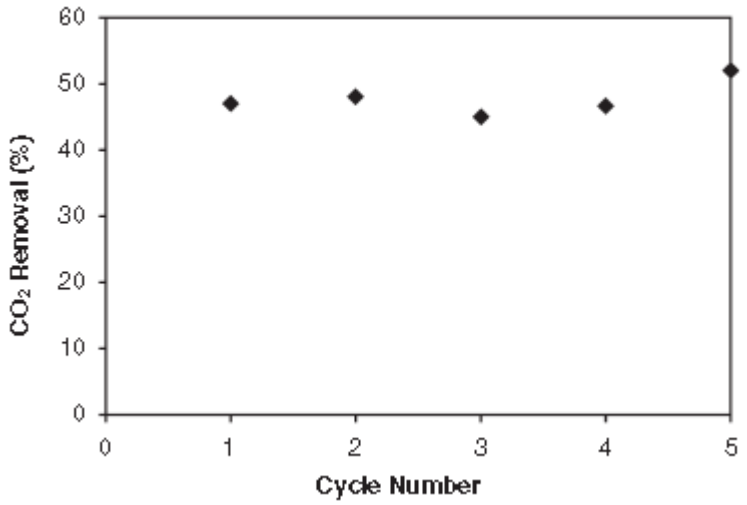

Figure 6.16. Results of the CO 2 removal efficiency from Ohio State University cyclic testing of calcium hydroxide at a Ca:C molar ratio of 0.75.

One of the main difficulties associated with the process is solids handling. Lime, limestone, and calcium hydroxide are all cohesive particles. Sorbent attrition and agglomeration, and electrostatic charge effects can cause operational difficulty. This is specifically true in the case of calcium hydroxide because of its natural particle size (D_{50} < 10 μm) and tendency to form a cementitious solid when exposed to low moisture concentrations. However, OSU has developed techniques to ensure proper feeding and flow of sorbent through the reactor system. Figure 6.15 shows the inside of the U - bend

section of the test loop. The figure shows that the section is clear from any sorbent clogging after a week of operation.

Another well - documented problem with using naturally occurring limestone is that the sorbent's ability to capture CO_2 decreases over multiple cycles. However, based on the single - cycle study with a hydration step added in between each cycle, the results, shown in Figure 6.16, indicate that no decay in sorbent reactivity occurs over five cycles. 50 If limestone calcination occurs between 900 ° C and 1,200 ° C, the lime product will significantly such that carbon dioxide can no longer diffuse effectively into the pore volume of the calcium oxide particle; however, the hydration reaction still can be effective. Once regenerated into calcium hydroxide, the sorbent effectively can capture CO_2.

A similar process is being demonstrated at CANMET Energy Technology Center in Canada. The Ca:C molar ratios used for the CANMET Process range from 4 to 25. These molar ratios are significantly higher than those for the CCR Process, which can remove virtually all the CO_2 in the flue gas stream with a Ca:C molar ratio of 1.5 and a residence time on the order of a second. It is thus expected that, compared with the CCR Process, the CANMET Process will require higher solids circulation and higher parasitic energy consumption for a given rate of the CO_2 removal.

6.3. Chemical Looping Gasification Integrated with Fuel Cells

The high efficiencies and flexibility to produce desired products, coupled with the integrated environmental benefits in terms of a readily sequestrable CO_2 stream, make chemical looping gasification of coal an attractive technology for energy conversion and management. The Coal - Direct Chemical Looping (CDCL) Process is very attractive because it is capable of converting as much as 80% of the thermal energy of coal into hydrogen. Here, energy conversion schemes that effectively extract chemical energy from the fuels are proposed by integrating the fuel cell with chemical looping.

6.3.1. Chemical Looping Gasification Integrated with Solid-Oxide Fuel Cells

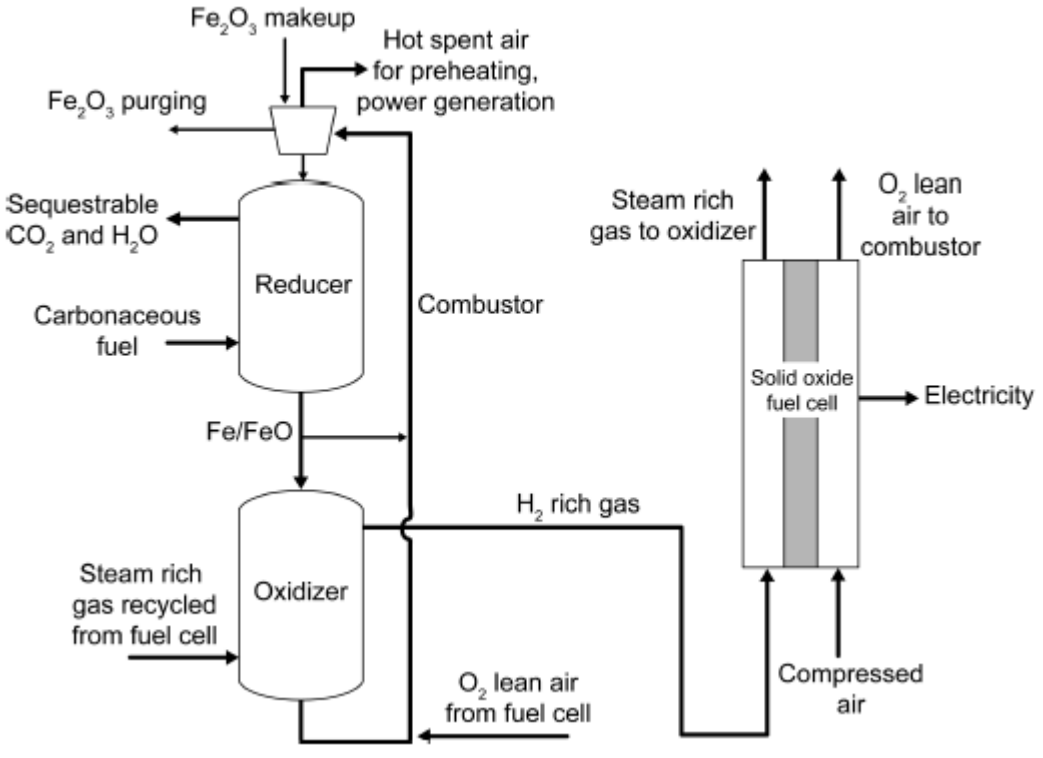

Figure 6.17. Chemical looping gasification integrated with a solid - oxide fuel cell.

Figure 17 illustrates an electricity generation scheme in which a chemical looping gasification system is integrated strategically with commercial solid - oxide fuel cells (SOFC) to minimize the exergy loss.

Under this configuration, the hydrogen - rich gas produced from the chemical looping oxidizer is introduced directly to the SOFC anode side for power generation. The exhaust of the SOFC anode, which is a hydrogen lean gas with a significant amount of steam, is recycled back to the chemical looping oxidizer for hydrogen generation. As shown in the figure, a closed loop between the chemical looping oxidizer and the SOFC anode is formed through the circulation of the gaseous mixture of steam and H_2 . The steam and H_2 mixture essentially acts as a " working fluid " for power generation. Although some recompression, purging, and makeup may be required for the working fluid, most steam is being circulated in the closed loop and will not be condensed. Therefore, steam condensation and reheating, a step that leads to significant exergy loss in the conventional power generation processes, can be minimized. The integration of the chemical looping oxidizer and the SOFC anode also eliminates the need for a gas turbine, which is required in a typical SOFC combined - cycle system. To enhance process efficiency, the chemical looping combustor can be configured such that the oxygen - lean exhaust air from the SOFC cathode is used to combust the Fe_3O_4 to Fe_2O_3. By doing so, the output of the high - grade heat is increased and the compression work for the air is reduced.

Table 6.1 Coal - to - Electricity Process Confi gurations and Process Efficiencies

Process Configuration	Conventional IGCC	CDCL–Combined Cycle	CDCL–SOFC
Efficiency (%HHV)	30–35	47–53	64–71
CO_2 Capture Rate (%)	90	100	100

Table 6.1 compares the efficiencies of the conventional IGCC process, the CDCL combined cycle, and the CDCL integrated with SOFC. As shown in the table, the CDCL – SOFC scheme has the potential of doubling the efficiency of state - of - the - art power generation processes. The significantly improved energy conversion efficiency results from the advanced energy integration scheme between chemical looping and the SOFC.

6.3.2. Direct Solid Fuel Cells

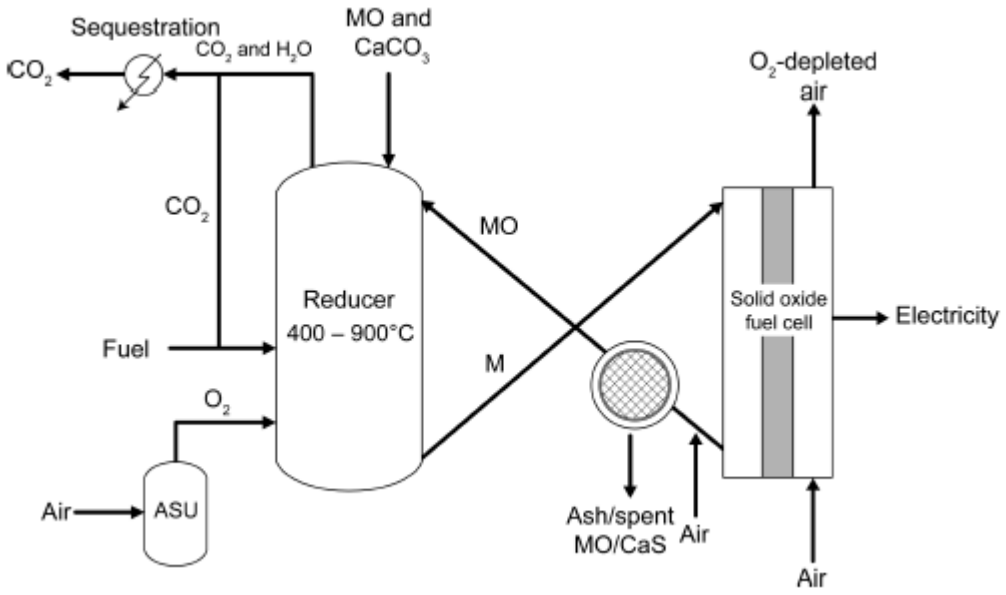

Figure 6.18. Direct solid - oxide fuel cell applications for chemical looping.

A more advanced electricity generation scheme includes the integration of a chemical looping reducer and a direct solid fuel cell. By modifying the electrochemical oxidation of supported Fe to supported Fe_2O_3 , thus generating electricity, a system integrating a chemical looping reducer and a direct solid fuel cell can be developed as illustrated in Figure 18.
In this scheme, reduced metal particles are fed directly into a solid - oxide fuel cell that can process solids directly. Particles are reduced in the fuel reactor and then introduced to the fuel cell to react with oxygen or air at 500 – 1,000°C to produce electricity. The oxidized particles are recycled back to the fuel reactor to be reduced again. It is desirable for particles to be conductive when metal is at both the oxidized and the reduced states.

The Ohio State University (OSU), led by L.-S. Fan, and the University of Akron (UA), led by S.S.C. Chuang, are developing chemical looping solid-oxide fuel-cell systems. The preliminary study of the solid - oxide fuel cell at UA indicates that the reduced Fe on Fe–Ti–O can serve as a fuel, producing 45 mA/cm 2 at 0.4 V and 800°C. The resultant oxidized Fe–Ti–O composite remained in the powder form and did not adhere to the anode surface of the fuel cell. The results suggest that an integrated fuel cell with chemical looping could be a viable approach for generation of electricity and a nearly pure CO_2 stream from coal.

The step for the generation of the electricity from Fe on Fe – Ti – O involves the following reactions:

Cathodic $O_2+4e^- \rightarrow 2O^{2-}$

Anodic $2Fe+3O^{2-} \rightarrow Fe_2O_3+6e^-$

The overall reaction corresponds to an ideal cell potential (i.e., open - circuit voltage) of 0.996 V at 800 ° C. The overall reaction is:

$2Fe+3/2O_2 \rightarrow Fe_2O_3$ $\Delta G=384$ KJ/mol

Table 6.2. The Ideal Cell Potentials (Open - Circuit Voltage)

		700°C		800°C		900°C	
	n	ΔG (kJ)	E (V)	ΔG (kJ)	E (V)	ΔG (kJ)	E (V)
$2Ni + O_2 \rightarrow 2NiO$	4	310	0.803	290	0.751	270	0.699
$4Cu + O_2 \rightarrow 2Cu_2O$	4	220	0.570	200	0.518	180	0.466
$4/3Fe + O_2 \rightarrow 2/3Fe_2O_3$	4	407	1.053	384	0.996	363	0.941
$2Fe + O_2 \rightarrow 2FeO$	4	405	1.049	390	1.010	370	0.958
$3/2Fe + O_2 \rightarrow 1/2Fe_3O_4$	4	405	1.049	390	1.010	370	0.958

The observation of electricity generation from the Fe – Ti – O composite indicates that the O_2 − can reach the reduced Fe to carry out the anodic reaction. Because this is one of the first attempts at using solid metal as the fuel for the fuel cell, the results appear promising. This direct solid fuel cell concept can be extended to other types of oxygen carriers such as Ni and Cu. Table 6.2 compares the ideal cell potentials of using these metals as fuels. Fe/Fe_2O_3 is the oxygen carrier that gives the highest ideal cell potential. CuO is not included, because it is not stable at 800 ° C; therefore, it will not be effective for coal chemical looping. Examining the anodic reaction suggests the need to build a pathway to facilitate the electrochemical oxidation of supported Fe.

Compared with the chemical looping – SOFC system, the direct solid fuel cell scheme is more challenging because of the relatively immature direct solid fuel cell technology. For the successful development of this direct solid fuel cell, the following issues need to be addressed.

1. The effectiveness of the direct solid fuel cell for generating electricity by using the supported Fe as a fuel.

2. The effectiveness of the supported Fe_2O_3 produced from the fuel cell for reaction with coal in the chemical looping process. The overall potential of integrating a fuel cell with chemical looping for electric power generation should continue to be evaluated in more detail.

6.4. Enhanced Steam Methane Reforming

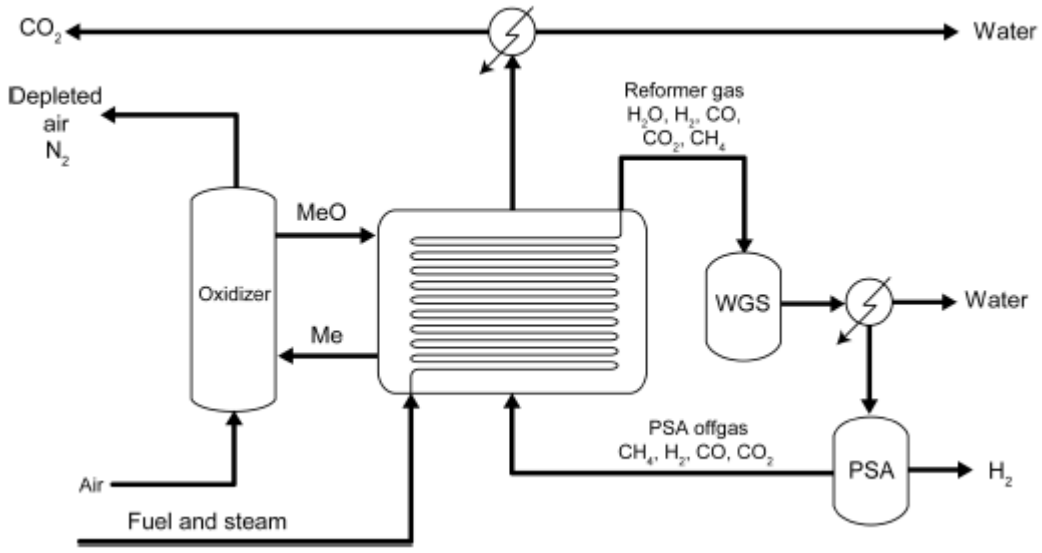

Figure 6.19. Schematic flow diagram of the chemical looping combustion integrated with the steam methane-reforming process (CLC – SMR).

Chemical looping combustion integrated with the steam methane reforming process (CLC – SMR) was studied by Rydén and Lyngfelt at Chalmers University of Technology in Sweden. The utilization of chemical looping combustion (CLC) in steam methane reforming (SMR) represents another potential application for the chemical looping strategy. A schematic flow diagram of the CLC – SMR Process is shown in Figure 6.19 . The CLC – SMR Process uses a combustor that is identical to that used in the CLC Process. The CLC – SMR Process also uses a reducer that is unique in that it integrates the function of the reducer used in the CLC Process to that of a reformer. The integrated reducer/reformer reactor is composed of a low - velocity bubbling fluidized bed with reformer tubes that are placed inside the reactor. The tubes are filled with reforming catalysts and behave as fixed - bed reactors. In the operation of the reformer, steam and methane are introduced into the reformer tubes at a ratio of ~ 3:1. By maintaining the reformer tubes at desirable reaction temperatures, typically 700 – 950°C, the methane is reformed into syngas, which is subsequently converted to hydrogen. This hydrogen stream is then purified through the WGS reaction and pressure swing adsorption (PSA) in the units downstream in the process.

The SMR reaction is highly endothermic as is the reduction reaction of the oxygen carrier particles in the reducer. Both reactions take place in the reducer/reformer reactor. The oxygen carrier reduction reaction occurs exterior to the reformer tube, whereas SMR occurs inside the reformer tube. The fuel for the oxygen carrier reduction

is the PSA tail gas and recycled methane. The reduction reaction product gases, CO_2 and steam, then exit the reducer. The reduced oxygen carrier particles are transported from the reducer to the combustor, where they are oxidized with air. The high - temperature particles resulting from the exothermic oxidation reaction provide the necessary heat for reduction and reforming reactions in the reducer/reformer reactor. In the CLC – SMR Process, the CLC system is operated at atmospheric pressure, whereas the SMR reformer tubes are operated at typical reformer pressures (15 – 40 atm).

As shown, the methane - reforming reaction scheme in the CLC – SMR Process is practically identical to that in the traditional SMR Process with the exception of the heat integration scheme for the reformer. In the traditional SMR Process, the heat required for steam methane reforming is provided by combustion of the fuel exterior to the reformer tubes. In contrast, the CLC – SMR Process uses high-temperature oxygen carrier particles as a heat transfer medium.

To date, the studies on this novel scheme have been limited to theoretical analysis such as heat and mass balances. Experimental testing results are not yet available. Theoretical analysis indicates that the CLC – SMR Process has the potential to achieve a higher H_2 yield than the conventional SMR Process. Therefore, it offers a viable approach for an innovative reforming operation. Some challenges, however, still exist for this process as illustrated below.

1. Approximately 70% of the methane is reformed and converted to H_2 and CO_2 in the WGS reactors. Thus, most of the carbon in this process is separated by the traditional methods such as PSA rather than CLC. Although all of the carbon in the feedstock exits from the reducer/ reformer, the CLC system is used to separate only approximately 30% of the total carbon in this process. Thus, the energy savings through carbon capture using the CLC system may not be significant.

2. Both the SMR reaction and the oxygen carrier particle reduction reaction, when nickel - or iron - based oxygen carriers are used, are highly endothermic. Thus, the heat required in the integrated reducer/reformer reactor will even be higher than that required in the traditional SMR reformer. The large heat requirement renders the heat integration in the CLC – SMR Process a challenging task.

3. Because high - temperature oxygen carrier particles are the sole heat carrier in the integrated reducer/reformer reactor, there will be a large solids circulation rate and likely a large temperature difference between the combustor and the reducer/reformer. An estimated solids circulation rate of 6,700 t/h for a 300 - MWth CLC – SMR Process indicates a significant solid flow rate issue.

4. Heat transfer using fluidized oxygen carrier particles could pose an increased erosion problem on the reformer tubes.

6.5. Tar Sand Digestion via Steam Generation

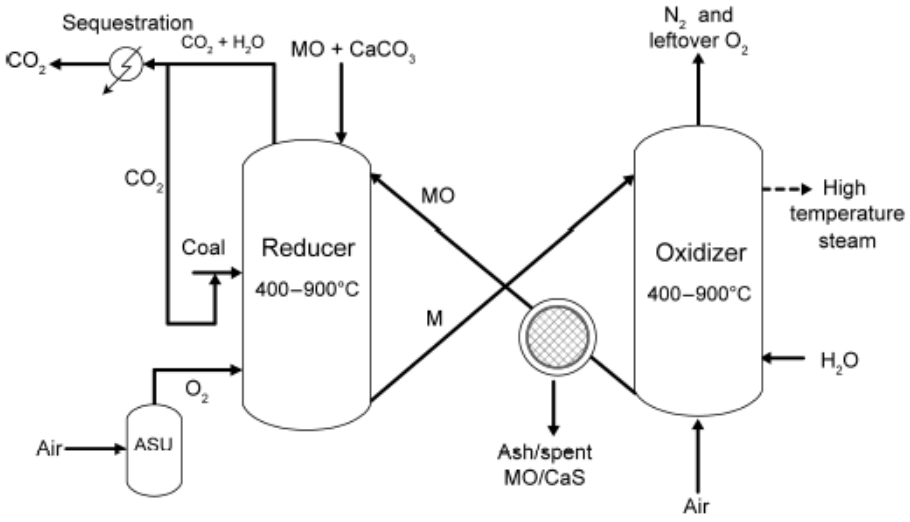

Figure 6.20: Heat and steam generation by the looping process.

In addition to producing hydrogen, reduced metal particles can be burned with air in an oxidation reactor, and the heat generated could be extracted using water to generate high - temperature steam. Figure 6.20 shows heat and steam generation by the chemical looping process. The steam could be used either for electricity generation or for various industrial applications. For example, steam can be used to extract heavy oil from tar sands. Providing steam via chemical looping technology is attractive for tar sand digestion, because less carbon is emitted throughout the overall process. This will better allow for this abundant energy source to be tapped with signifi cantly reduced greenhouse gas emissions.

6.6. Liquid Fuel Production from Chemical Looping Gasification

Even beyond hydrogen, heat, and electricity generation the chemical looping gasification strategy can be used to achieve liquid fuel synthesis with high yield and low exergy loss. The chemical looping gasification system produces CO_2 , H_2 , and heat/power from the carbonaceous fuel. The heat and power produced compensate for the parasitic energy requirements. Under this scheme, part of the CO_2 generated from the reducer is sequestered, while the remaining CO_2 reacts with H_2 generated from the oxidizer in a reactor that simultaneously performs the reverse WGS and Fischer – Tropsch (F – T) reactions:

$CO_2+H_2 \leftrightarrow CO+H_2O$

$CO+2H_2 \leftrightarrow -(CH_2)- +H_2O$

The Fischer – Tropsch reaction of this type, also called CO_2 hydrogenation, has been studied since the 1990s to identify novel applications of CO_2 for greenhouse gas control. It was determined based on these studies that such an F – T reaction is feasible when an iron - based F – T catalyst is used.

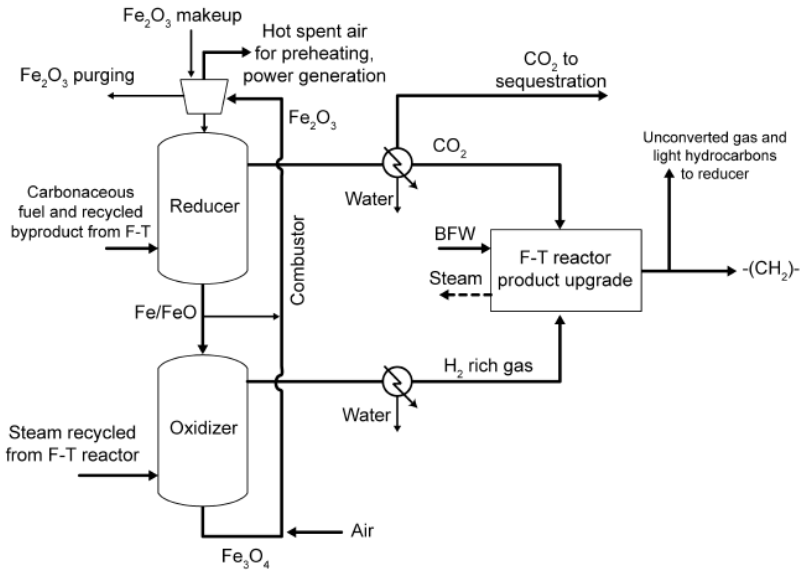

Figure 6.21. Chemical looping gasifi cation for liquid fuel synthesis

Compared with the conventional CTL processes, the chemical - looping - based reaction scheme given in Figure 6.21 has several distinct advantages.

1. The unique chemical looping gasification strategy effectively gasifies the fuel with minimal exergy loss.

2. Both the endothermicity of the fuel gasification reactions and the exothermicity of the F – T reaction are reduced; moreover, the F – T by - products such as steam and unconverted fuel are readily used in the chemical looping gasification system. Therefore, the exergy loss for the overall process is reduced further via an improved energy management scheme.

3. The fuel gasification and pollutant control schemes are simpler. For example, the elaborate partial syngas shift, COS hydrolysis, and acid gas separation steps in the conventional indirect CTL process are avoided.

4. The CO_2 by - product is concentrated and readily sequestrable. A case study is performed to evaluate the exergy loss of the conventional CTL process and the chemical - looping - gasification - based CTL process.

Table 6.3. Performance Comparisons of Conventional CTL and Chemical -Looping - Gasifi cation - Based CTL

	Conventional CTL	Chemical Looping-CTL
Exergy Loss (MW)[a]	835	**503**
Marginal Change in Exergy Loss (%)	n/a	**–39.8**

[a]For an 80,000-bbl/d (36,288-kg/d) plant.

The results are given in Table 6.3 . As shown in the table, through the utilization of the chemical looping gasification strategy, the exergy loss of the CTL process can be reduced by nearly 40%. Thus, the novel chemical - looping - based liquid fuel synthesis scheme has the potential to improve significantly the efficiencies of conventional CTL processes.

6.7. Chemical Looping with Oxygen Uncoupling (CLOU)

To combust carbonaceous fuels with metal oxide oxygen carriers, the chemical looping with oxygen uncoupling (CLOU) Process, initiated by Lewis and Gilliland and extensively tested at the Chalmers University of Technology, uses a reaction scheme different from that of the typical chemical looping process discussed thus far. The oxygen carrier in the reducer of a typical chemical looping process releases its oxygen directly through a reduction reaction with the fuel. In contrast, the oxygen carrier in the reducer of a CLOU Process releases the oxygen through decomposition to form molecular gaseous oxygen, which then oxidizes the fuels. When the CLOU reaction scheme is implemented, it yields a more effective process in oxidizing, particularly, the solid fuels in the reducer than does the typical chemical looping processes. The specific reactions that take place in CLOU include:

$Me_xO_y \rightarrow Me_xO_z+(y-z)/2O_2$

$C_nH_{2m}+(n+m)/2O_2 \rightarrow nCO_2+mH_2O$

$Me_xO_z+(y-z)/2O_2 \rightarrow Me_xO_y$

The first two reactions occur in the reducer, and the third reaction occurs in the oxidizer. For the first two reactions to occur effectively, the equilibrium partial pressure of the oxygen be high at the reaction temperature. This unique requirement narrows the potential options for oxygen carriers. Three metal oxides satisfy this requirement; they are CuO, Mn_2O_3, and Co_3O_4.

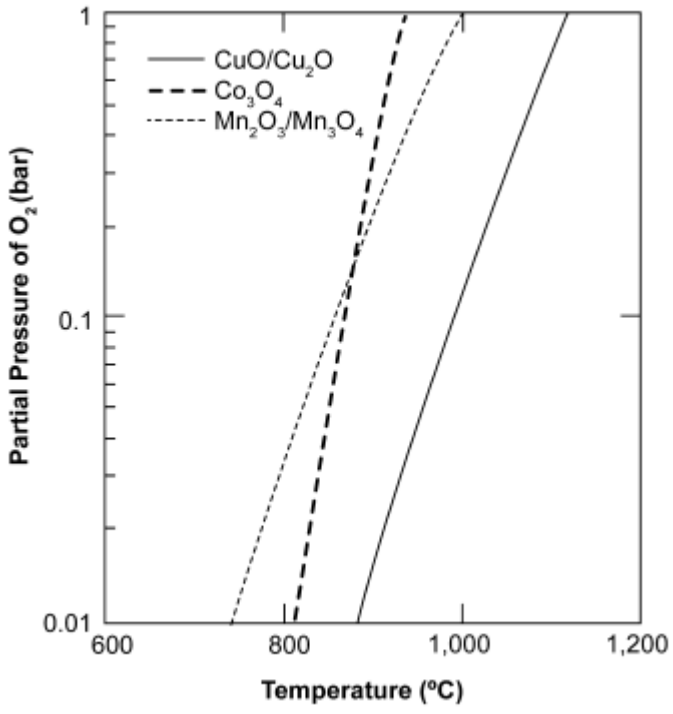

Figure 6.22. Partial pressure of gas-phase O2 over metal - oxide systems as a function of temperature. CuO/Cu2O (—); Co3O4 /CoO (– – –) Mn2O3 /Mn3O4 (- - -).

The equilibrium oxygen partial pressures for these three metal oxides as a function of temperature are given in Figure 6.22 . It is shown that an increase in temperature leads to an increase in the oxygen partial pressure. When the heat of reaction for both Reactions (first and second), is considered, the reactions of the metal oxides CuO/Cu_2O and Mn_2O_3/Mn_3O_4 with the fuel are exothermic and are thus more suitable for CLOU than the reaction of metal oxide Co_3O_4/CoO with the fuel that is endothermic. Exothermic reactions are beneficial as the oxygen decomposition is enhanced with an increase in temperature.

Mattisson tested the CLOU Process for methane conversion using a copper - based oxygen carrier of 125 – 180 µm, synthesized by freeze granulation at 60% CuO and 40% ZrO_2. The test was performed in a 30 - mm - ID quartz fluidized - bed reactor operated under batch mode with reduction and oxidation carried out by turns in the same reactor. Nitrogen gas was used between the oxidation and reduction steps to prevent any mixing of gases. The total mass of the oxygen carrier used was 10 g, and the fuel flow rate was 600 mL/min. The experiment was performed at 950 ° C. The results indicate that the oxygen carrier decomposition changes with the reactor temperature during the reduction step. During the oxidation step, the CO/CO_2 peaks were identified at the initial stage of air oxidation. This result reveals the deposition of carbon, which only occurs in the presence of metallic copper. It was therefore concluded that the CuO - based oxygen carrier was reduced to metallic copper during the reduction step.

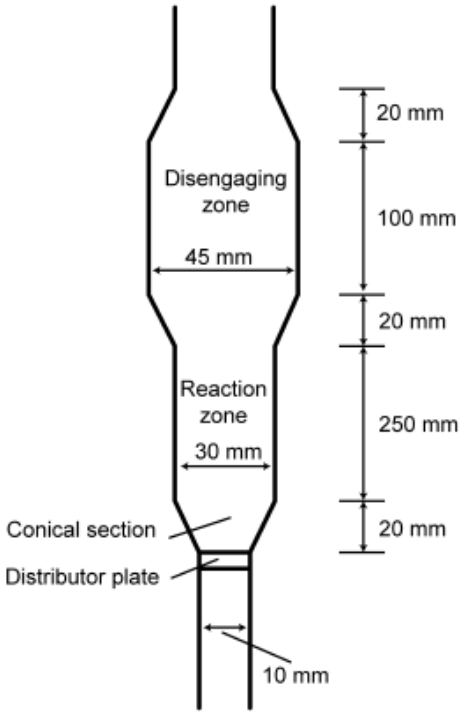

Figure 6.23. Laboratory fluidized - bed reactor used for solid - fuel CLOU testing by Chalmers University.

After the gaseous fuel testing, studies using various solid fuels were conducted using a laboratory fluidized bed reactor, as shown in Figure 23 . In the figure, a conical section above the distributor plate was used to provide proper mixing of the solid fuel and the oxygen carrier. A disengaging zone above the reaction zone prevented the entrainment of small particles from the bed. In all the solid fuel tests, 15 g of oxygen carrier was used and 0.1 g of solid fuel was introduced during each reduction cycle. The size range of the fuel, that is, 180 – 250 μm, is slightly greater than that of the oxygen carrier. The gas flow rate during oxidation and reduction was maintained at 900 mL/min for the air and nitrogen flows.

Mattisson used a copper - based oxygen carrier (40% CuO and 60% ZrO_2) of 125 – 180 μm, synthesized by freeze granulation, to determine the rate of conversion of petroleum coke. Experiments were designed to study the influence of the reducer temperature on the conversion rate of petroleum coke. The results indicated a strong dependence of the conversion rate of petroleum coke on the reducer temperature. The time for 95% decreased from 130 s to 20 s with an increase in temperature from 885 ° C to 985 ° C. A similar conversion of petroleum coke was observed after 15 minutes when iron - based oxygen carriers were used in a typical CLC scheme, highlighting the significant conversion rate observed while using the CLOU scheme. Leion tested the conversion rates for six different solid fuels using the copper - based oxygen carrier.

Table 6.4. Solid Fuels Testing Results Using the CLOU Concept: Copper-BasedMetal Oxide vs. Iron-Based Metal Oxide

	Mexican Petroleum Coke		South African Coal		Indonesian Coal	
Type of Fuel	CLOU	CLC	CLOU	CLC	CLOU	CLC
Time for 95% Conversion (s)	41	648	40	612	30	282
Rate of 95% Conversion (%/s)	2.3	0.15	2.4	0.16	3.2	0.34
	Columbian Coal		German Lignite		Swedish Wood Char	
Type of Fuel	CLOU	CLC	CLOU	CLC	CLOU	CLC
Time for 95% Conversion (s)	51	606	25	84	28	378
Rate of 95% Conversion (%/s)	1.9	0.16	3.8	1.13	3.4	0.25

The results were compared with those when the CLC scheme is used, and the outcome is summarized in Table 4 . All the experiments were carried out at 950 ° C. The oxidation of the oxygen carriers was carried out using 10% O_2 balanced with nitrogen. The table highlights the increased reaction rates observed when adapting the CLOU

scheme for solid fuels. Leion also stated that the methane and CO emissions from the CLOU process are lower than those observed in the typical CLC process. The activity involving CLOU testing using metal oxides other than copper oxide is limited. The application of the copper - based oxygen carrier is, however, constrained because of the low melting point of copper. Furthermore, as the extent of decomposition of copper oxide is low, a very high circulation rate of copper oxide is thus required for process applications. So far, the only testing performed has been in a laboratory - scale fluidized - bed reactor.

6.8. Concluding Remarks

This section presents examples of novel applications of chemical looping processes for H_2 storage and onboard H_2 production, CO_2 capture in combustion flue gas, power generation using fuel cells, SMR, tar sand digestion, and liquid fuel production. Each application employs a unique feature of the chemical looping strategy that characterizes process intensification, leading to a highly efficient process system. In these particular applications, metal oxide can be used to assist in tar sand digestion and steam methane reforming. The reduced metal oxide from the reducer can be used for the following applications: onboard H_2 production by reacting it with steam, power production by combusting reduced metal oxide in the fuel cell anode, and generation of steam or heat by reacting it with air. In processes such as CLOU, the metal oxide, instead of being reduced by the fuel, can be decomposed to yield molecular gaseous oxygen in the reducer at a high temperature. It is followed, in the reducer, by combustion of molecular gaseous oxygen with fuel to form CO_2 and steam. When this reaction scheme is implemented, the CLOU process is more effective in combusting the gaseous or solid fuels in the reducer than does the typical chemical looping process. The use of the calcium sorbent for CO_2 capture through the carbonation – calcination – hydration looping reactions provides a high - temperature, sorbent - based CO_2 separation method that is a viable alternative to the traditionally low - temperature, solvent - based separation methods. All these chemical looping examples represent energy conversion systems on the cutting edge of efficiency and technology where CO_2 separation, pollutant control, and product generation can be achieved readily. Employing the fundamental chemical looping concept, other chemical looping schemes also can be conceived, leading to highly efficient process applications.

References

A.Lyngfelt, M.Johansson ; T.Mattisson: CHEMICAL LOOPING COMBUSTION - STATUS OF DEVELOPMENT. (2008)

ASPEN technology, Inc.: Getting Started Modeling Processes with Solids.

Cao, Yan ; Pan,Wei-Ping: Investigation of Chemical Looping Combustion by Solid Fuels. 1.Process Analysis. (2006)

Fan, L.: Chemical looping systems for fossil energy conversion. John Wiley and Sons, Inc., Hoboken, New Jersey, 2010

Juan Adanez, Luis F. de Diego Pilar Gayán Javier C. ; Abad, Alberto: CHARACTERIZATION OF OXYGEN CARRIERS FOR CHEMICAL-LOOPING COMBUSTION.

Burke , A. F. , and M. Gardiner , " Hydrogen Storage Options: Technologies and Comparisons for Light - Duty Vehicle Applications , " UCD - ITS - RR - 05 - 01, Institute of Transport Studies, University of California, Davis (2005).

Akiba , E. , " Research and Development of Hydrogen Storage Technologies," *Journal of the Japan Institute of Energy* , 85 (7), 510 – 516 (2006).

Heung , L. K. , and G. G. Wicks , " Silica Embedded Metal Hydrides, " *Journal of Alloys* and Compounds , 293 – 295 , 446 – 451 (1999).

Bogdanovic , B. , and M. Schwickardi , " Ti - doped NaAlH 4 as a Hydrogen – Storage Material – Preparation by Ti - Catalyzed Hydrogenation of Aluminum Powder in Conjunction with Sodium Hydride , " Applied Physics A , (72), 221 – 223 (2001).

Heung , L. K. , " Using Metal Hydride to Store Hydrogen , " U.S. Department of Commerce, National Technical Information Service, Springfi eld, VA (2003).

Browman , R. C. , Jr ., S. - J. Hwang , C. C. Ahn , and J. J. Vajo , NMR and X - ray Diffraction Studies of Phases in the Destabilized LiH - Si System , Materials Research Society Symposium Proceedings, 837, N3.6.1 – N3.6.6 (2005).

Li , S. , and P. Jena , Electronic Structure and Hydrogen Desorption in NaAlH 4 , Materials Research Society Symposium Proceedings, 837, N2.5.1 – N2.5.8 (2005).

Bruster , E. , T. A. Dobbins , R. Tittsworth , and D. Anton , Decomposition Behavior of Ti - Doped NaAlH 4 Using X - Ray Absorption Spectroscopy at the Titanium K - Edge, Materials Research Society Symposium Proceedings, 837, N3.4.1 – N.3.4.6 (2005).

Araujo , C. M. , R. Ahuja , and J. M. O. Guillen , " Role of Titanium in Hydrogen Desorption in Crystalline Sodium Alanate , " *Applied Physics Letters* , 86 (25), 251913 1 – 3 (2005).

Schuth , F. , B. Bogdanovic , and M. Felderhof , " Light Metal Hydrides and Complex Hydrides for Hydrogen Storage , *" Chemical Communications* , 24 , 2249 – 2258 (2004).

Garberoglio , G. , A. I. Skoulidas , and J. K. Johnson , " Adsorption of Gases in Metal Organic Materials: Comparison of Simulations and Experiments , " *Journal of Physical Chemistry B* , 109 (27), 13094 – 13103 (2005).

Rosi , N. L. , J. Eckert , M. Eddaoudi , D. T. Vodak , J. Kim , M. O' Keeffe , and O. M. Yaghi ., " Hydrogen Storage in Microporous Metal - Organic Frameworks , " *Science*, 300 , 1127 (2003).

Jung , D. H. , D. Kim , T. B. Lee , T Lee , S. B. Choi , J. H. Yoon , J. Kim , K. Choi , and S. - H. Choi , " Grand Canonical Monte Carlo Simulation Study on the Catenation Effect on Hydrogen Adsorption onto the Interpenetrating Metal – Organic Frameworks , " *Journal of Physical Chemistry B* , 110 (46), 22987 – 22990 (2006).

Li , Y. , F. H. Yang , and R. T. Yang , " Kinetics and Mechanistic Model for Hydrogen Spillover on Bridged Metal − Organic Frameworks , " *Journal of Physical Chemistry C* , 111 (8), 3405 – 3411 (2007).

Li , Y. , and R. T. Yang , " Hydrogen Storage in Metal − Organic Frameworks by Bridged Hydrogen Spillover , " *Journal of the American Chemical Society* , 128 (25), 8136 – 8137 (2006).

Dillon , A. C. , J. L. Blackburn , P. A. Parilla , Y. , Zhao , Y. - H. Kim , S. B. Zhang , A. H. Mahan , J. L. Alleman , K. M. Jones , K. E. H. Gillbert , et al. *Discovering the Mechanism of H2 Adsoprtion on Aromatic Carbon Nanostructures to Develop Adsorbents for Vehicular Applications* , Materials Research Society Symposium Proceedings, 837, N4.2.1 – N4.2.7 (2005).

Lee , Y. W. , R. Deshpande , A. C. Dillon , M. J. Heben , H. Dai , and B. M. Clemens , *The Role of Metal Catalyst in Near Ambient Hydrogen Adsorption on Multi – walled Carbon Nanotubes* , Materials Research Society Symposium Proceedings, 837, N3.18.1 – N3.18.6 (2005).

Wang , Y. , and Z. Iqbal , *Electrochemical Hydrogen Adsorption/Storage in Pure and Functionalized Single Wall Carbon Nanotubes* , Materials Research Society Symposium Proceedings , 837 , N4.4.1 – N4.4.12 (2005).

Gupta , B. K. , R. S. Tiwari , and O. N. Srivastava , " Studies on Synthesis and Hydrogenation Behavior of Graphite Nanofi bers Prepared through Palladium Catalyst Assisted Thermal Cracking of Acetylene , " *Journal of Alloys and Compounds* , 381 , 301 – 308 (2004).

Ahn , C. C. , Y. Ye , B. V. Ratnakumar , C. Witham , R. C. Bowman , and B. Fultz , " Hydrogen Desorption and Adsorption Measurements on Graphite Nanofi bers , " *Applied Physics Letters* , 73 , 3378 – 3380 (1998).

Fan , Y. - Y. , B. Liao , M. Liu , Y. - L. Wei , M. - Q. Lu , and H. - M. Cheng , " Hydrogen Uptake in Vapor - Grown Carbon Nanofi bers , *" Carbon* , 37 , 1649 – 1652 (1999).

Hong , S. E. , D. – K. Kim , S. M. Jo , D. Y. Kim , B. D. Chin , and D. W. Lee , " Graphite Nanofi bers Prepared from Catalytic Graphitization of Electrospun Poly(Vinylidene Fluoride) Nanofi bers and Their Hydrogen Storage Capacity , " *Catalysis Today* , 120 ,413 – 419 (2007).

Lee , K. B. , A. Verdooren , H. S. Caram , and S. Sircar , " Chemisorption of Carbon Dioxide on Potassium - Carbonate - Promoted Hydrotalcite , " *Journal of Colloid and Interface Science* , 308 , 30 – 39 (2007).

Fan , L. - S. , and H. Gupta , " Sorbent for the Separation of Carbon Dioxide (CO 2) from Gas Mixtures, " U.S. Patent 7,067,456 (2006).

Sun , P. , C. J. Lim , and J. R. Grace , " Cyclic CO 2 Capture by Limestone – Derived Sorbent During Prolonged Calcination/Carbonation Cycling , " *AIChE Journal* , 54 , 1668 – 1677 (2008).

Fan L. - S. , S. Ramkumar , W. Wang , and R. Statnick , " Separation of Carbon Dioxide from Gas Mixtures by Calcium Based Reaction Separation Process, " Provisional Patent Application No. 61/116,172 (2008).

Jin , H. , and M. Ishida , " A New Type of Coal Gas Fueled Chemical – Looping Combustion ," *Fuel* , 83 , 2411 – 2417 (2004).

Gupta , P. , L. G. Velazquez - Vargas , T. Thomas , and L. - S. Fan , *Process of Chemical Looping Combustion of Coal* , 30 th Proceedings of the 30th International Technical Conference on Coal Utilization & Fuel Systems, Clearwater, Florida, April 17 – 21 , (2005).

Garcia - Labiano , F. , J. Adanez , L. F. de Diego , P. Gayan , and A. Abad , " Effect of Pressure on the Behavior of Copper - , Iron - , and Nickel - Based Oxygen Carriers for Chemical - Looping Combustion , " *Energy & Fuels* , 20 (1), 26 – 33 (2006).

Kronberger , B. , A. Lyngfelt , G. Loeffler , and H. Hofbauer , " Design and Fluid Dynamic Analysis of a Bench - Scale Combustion System with CO 2 Separation − Chemical - Looping Combustion , " *Industrial & Engineering Chemistry Research* , 44 (3), 546 – 556 (2005).

Fan , L. - S. , F. L i, L. Zeng , and D. Sridhar , " Integration of Reforming/Water Splitting and Electrochemical Systems for Power Generation with Integrated Carbon Capture " , Provisional Patent Application Number 61/240,508 (2009).

Chuang , S. S. C. , " Catalysis of Solid Oxide Fuel Cell , " *Catalysis* , 18 , 186 – 198 (2005)

Chuang , S. S. C. , " Coal- Based Fuel Cell, " WO 2,006,028,502 (2006).

Ryden , M. , and A. Lyngfelt , " Using Steam Reforming to Produce Hydrogen with Carbon Dioxide Capture by Chemical - Looping Combustion , " *International Journal of Hydrogen energy* , 31 (10), 1271 – 1283 (2006).

Riedel T. , M. Claeys , H. Schulz . , G. Schaub , S. S. Nam , K. W. Jun , M. J. Choi , G. Kishan , and K. W. Lee , " Comparative Study of Fischer - Tropsch Synthesis with H 2 /CO and H 2 /CO 2 Syngas Using Fe - and Co - Based Catalysts , " *Applied Catalysis A - General* , 186 (1 – 2), 201 – 213 (1999).

Mattisson , T. , A. Lyngfelt , and H. Leion , " Chemical - Looping with Oxygen Uncoupling for Combustion of Solid Fuels , " *International Journal of Greenhouse Gas Control* , 3 (1), 11 – 19 (2009).

Leion , H. , T. Mattisson , and A. Lyngfelt , " Using Chemical - Looping with Oxygen Uncoupling (CLOU) for Combustion of Six Different Solid Fuels , " *Energy Procedia* , 1 , 447 – 453 (2009).

Chemical Engineering Journal Volume 236, 15 January 2014, Pages 121–130

Applied Energy Volume 113, Pages 1-1964 (January 2014)